Optimization of Whispering Gallery Mode Microsphere Resonators and Their Application in Biomolecule Sensing

By

Lin Zeng

Submitted to the graduate degree program in Chemistry and the Graduate Faculty of the University of Kansas in partial fulfillment of the requirements for the degree of Master of Science.

Chairperson: Dr. Robert C. Dunn

Dr. Cindy Berrie

Dr. Michael Johnson

Date Defended: December 15th, 2016

The Thesis Committee for Lin Zeng

certifies that this is the approved version of the following thesis:

Optimization of Whispering Gallery Mode Microsphere Resonators and Their Application in Biomolecule Sensing

Chairperson: Dr. Robert C. Dunn

Date approved: December 15th, 2016

Abstract

Optical Whispering gallery mode (WGM) resonators have attracted attention due to their label-free and sensitive detection capabilities for sensing. Light is confined and continuously recirculated within the cavity via total internal reflection at the resonant wavelength. The long recirculation time significantly enhances the interaction of light with sample, enabling improved sensitivity. Among various WGM resonators with different geometries, microsphere resonators fabricated with heating via surface tension can achieve ultrahigh quality factors and small mode volumes, making them good candidates for WGM sensing applications.

The sensing performance of a microsphere resonator is greatly related to its size. Therefore, the fabrication method is optimized to form silica microspheres with smooth surfaces and different sizes ($15\mu m$~$165\mu m$ in diameter). The size effects on their sensitivities and quality factors are studied. Silica microspheres with optimal sizes (~$45\mu m$ in diameter), which achieve high sensitivities and large quality factors, are selected for sensing applications. In addition, the thermal effect on WGM resonators is also explored for silica microspheres and barium titanate microspheres. WGM resonant wavelength shift versus temperature change is measured in a range of 21℃ to 45℃. Red shifts with increasing temperature are observed in all size microsphere resonators, which match the theoretical analysis.

Silica microsphere resonators with the optimal sizes are utilized in a WGM biomolecule sensing application. Cholera toxin specifically binds to GM1, which can be detected by the WGM resonant wavelength shift. A DOPC/GM1 bilayer is transferred onto the surface of a silica microsphere via the Langmuir-Blodgett technique. When cholera toxin molecules bind to GM1, the refractive index increases, leading to the red shift of the resonant wavelength. By changing the GM1 concentration in the DOPC/GM1 bilayer and measuring the total WGM shift, we find

the maximum amount of GM1 that can be coated onto a silica microsphere's surface to bind cholera toxin molecules.

Overall, the cavity size effect and thermal influence on WGM silica microsphere resonators are studied and optimized to achieve high sensitivities and high quality factors. As label-free optical detectors, silica microsphere resonators' application in biomolecule sensing is demonstrated.

Acknowledgements

I still remember the moment that I received the offer from KU. I was so excited because my dream finally came true. When I started to learn English in primary school, I knew there was a country called America. Since then I have had great interest in this developed country with beautiful scenery and advanced technologies. I always hoped I could have chance to see the real United States. These three and half years in America has been a wonderful journey. I have been so lucky to meet so many good people who have helped me a lot; I went to some beautiful cities, seeing a lot of famous architecture and scenery. In addition, I have become a more independent and responsible person. Before I came to America, I got used to relying on my parents for everything. If I met something difficult or I was unhappy, I always asked for their help. However, since I came to America, I have gradually grown up and become a more mature person. Now I can cook many different dishes; I can drive long distances by myself; and I have learned a lot of new things as well. Besides taking care of myself very well, I was also able to take care of my parents when they were in America.

I also feel so grateful that I could come to the Chemistry Department of KU and I was so lucky to join Dr. Dunn's group. Here, I'd like to briefly acknowledge some key individuals who gave me plenty of help during my graduate studies.

During the past three years, my advisor Dr. Dunn (Bob) provided me continuous support and encouragement, expanding my knowledge and scientific abilities. He is a very responsible and knowledgeable professor. I have learned a lot from him, not only scientific knowledge, but also independent thinking ability, problem solving skills and a responsible attitude, enabling me to become a better researcher. It was a really great experience to become Dr. Dunn's student, he has been and will always be my favorite mentor and teacher.

I would also like to acknowledge the help and support from the current and past members of the Dunn lab. I am very grateful for Dr. Sarah Wildgen's guidance and encouragement. She was super nice and patient; she was always willing to answer my various questions and provide very useful suggestions. She was also a good friend who comforted me when I was frustrated and unhappy. I also appreciate Dr. Daniel Kim's help. Daniel was a very smart and kind-hearted person. He helped me a lot with my experimental setup and computer issues, especially the laser aligning. I used to spend a day or even several days to align my laser, but now I can finish it in several hours, owing to Daniel's guidance. In addition, I would also like to thank the current group members Brittany DeWitt, Chess Volp and Brittany Sanders for their continuous help. As an international student, my English was not very fluent at the beginning, but they were always very patient when communicating with me and also helped me improve my writing skills.

Although I am alone in America, my parents and friends' support makes me never feel lonely. To my parents, thank you for understanding and encouraging me to pursue my dream. Thank you for raising me to be a responsible, kind and optimistic person, and telling me never to give up. Thank you to my cousin Zhehao Zhang, my only family in America. Every time when I was very frustrated about my experiment, it was very good to talk to you. Your optimistic attitude made me cheer up and gave confidence again. Thank you to Kavisha Ulapane, Katie Osborne, Yunan Wang, Yan Wang, Zhenyuan You, Yu Wang and Xiaomeng Su for being my good friends. Knowing you guys is one of the best things that happened to me in Lawrence. Thank you for letting me share my good times and hard times with you, and standing by my side all the time. Lastly, I'd like to thank everyone else who has also helped and supported me these years; you have made my life more colorful.

Table of Contents

List of Figures

List of Tables

Chapter 1

Whispering Gallery Mode Resonators

1.1 Introduction

Resonant optical sensors have drawn much attention, owing to their compact structure, wide dynamic range, electrical passiveness and various sensing capabilities. They have, for example, been used in the measurement of temperature, pressure, force, and biomolecules.[1] Among optical sensors, one specific category based on microcavities supporting whispering gallery modes (WGMs), has aroused interest due to their unique features such as high quality factor (Q-factor), small mode volume and label-free detection capabilities.[2] Historically, the whispering gallery mode phenomenon was first described by Lord Rayleigh in 1910, based on the observations of sound traveling the gallery in St. Paul's Cathedral in London. He explained that when two people faced away from each other at the opposite sides of the gallery, one could hear another's whisper via sound reflections along the circular wall.

In the beginning of the 20th century, scientists realized that a similar phenomenon could be observed for electromagnetic waves in small, circular symmetric dielectric cavities as well. Light propagates along a path around the cavity surface via continuous total internal reflection as a result of the refractive index differences between the surrounding medium and the resonator. This phenomenon has been named whispering gallery mode (WGM). Although WGM has been known for many years, the particular properties and various advantages still attract researchers' interests. The optimization of fabrication techniques has made it possible to fabricate microscale WGM resonators with larger Q-factor and higher sensitivity for sensing applications. Before discussing WGM sensors in details, it is necessary to discuss the concepts of total internal

reflection and the evanescent wave.

1.1.1 Total Internal Reflection and the Evanescent Wave

Whispering gallery mode resonances can be obtained by continuously recirculating light inside a resonator at the cavity interface via total internal reflection. Light transmission from one material to another is represented by Snell's law:

$$\boldsymbol{n_1 Sin\,\theta_1 = n_2\, Sin\,\theta_2} \qquad \textbf{Equation 1.1}$$

where n_1 and n_2 are refractive indexes of the two materials, and $\theta_1$and θ_2 are angles of the incident light and refracted light, as shown in **Fig. 1.1**. When light strikes the interface between two materials with different refractive indexes, the wave will be partially refracted and partially reflected. At small incident angles, light passing from a medium of higher refractive index to a medium of lower refractive index will be both refracted and reflected. By increasing the incident angle θ_1, the refracted angle θ_2 also increases. When $\theta_2 = 90°$, no light is refracted, instead it is all reflected. This θ_1 is defined as the critical angle θ_c:

$$\boldsymbol{\theta_c = sin^{-1}(\frac{n_2}{n_1})} \qquad \textbf{Equation 1.2}$$

As long as the incident angle θ_1 is equal to or greater than the critical angle θ_c, light is totally reflected back into the original medium instead of refracting into the low refractive index material, achieving total internal reflection (TIR), as shown in **Fig. 1.1**.

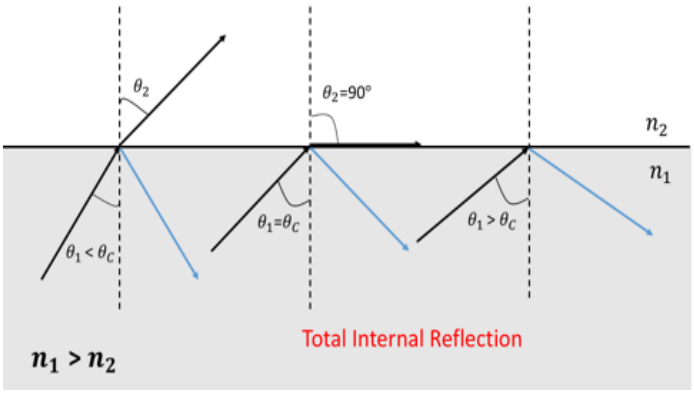

Figure 1.1. Light behavior at the interface between two media is described by Snell's law (equation 1.1). At small incident angles θ_1, light transferring from a higher refractive index medium (n_1) to a lower refractive index medium (n_2) will be refracted (θ_2) and partially reflected as well. At critical angle (θ_c), incident light is 100 % reflected back into the initial medium, with no refraction light, this phenomenon is called total internal reflection (TIR). As incident angle is larger than the critical angle, TIR occurs.

An important application of this is in optical fibers where light can be transmitted along its axis via TIR. The fiber consists of an inner core covered by a cladding layer, both materials are dielectric, and the outermost layer is plastic jacket. The refractive index of the core is greater than that of the cladding layer, causing the light to reflect off the boundary between the two layers. As a result, light is able to propagate through the fiber with a little loss.

When light transmitting through a medium undergoes TIR, evanescent waves, which are non-propagating, exponentially decaying electromagnetic fields are formed. Evanescent waves extend into the lower refractive index medium, as illustrated in **Fig. 1.2.** As visible light is totally reflected, the evanescent wave extends into the medium ~ 200 nm.[3] Crucially, this non-propagating field can interact with molecules at the medium surface, which provides a convenient method for label-free sensing platforms. For whispering gallery mode resonators,

light is captured inside the cavity via TIR, and the evanescent wave is an important component for WGM sensing applications.

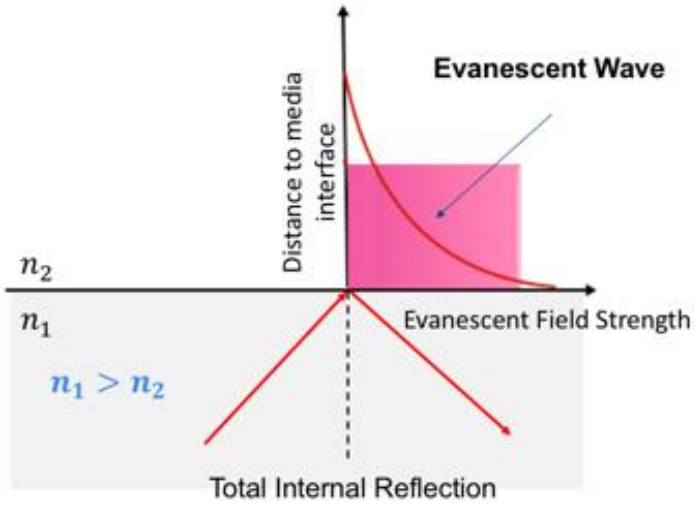

Figure 1.2. Formation of an evanescent wave at the media interface via total internal reflection (TIR). The evanescent field strength exponentially decays with the increasing distance D to media interface.

1.2 Whispering Gallery Mode Resonators

Common WGM resonators are made of dielectric, high refractive index materials and fabricated with smooth, circular cross sections that can confine light inside via nearly TIR at the boundary between the resonator and the surrounding medium. When the circumnavigation distance within the resonator is equal to an integer number of the coupled light wavelength, constructive interference occurs, leading to WGM resonances, as illustrated in **Fig. 1.3**.

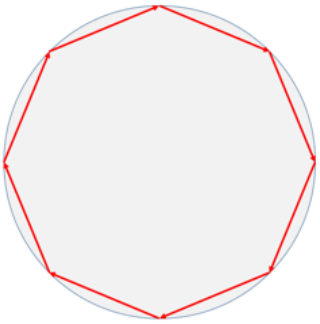

Figure 1.3. WGM resonance is achieved through continuous TIR within a spherical microcavity.

Light is able to propagate within WGM resonators when the refractive index of the resonator is greater than that of its surrounding medium. Resonance is achieved when the following criteria is realized:

$$\boldsymbol{\lambda_r = \frac{2\pi r n_{eff}}{m}} \qquad \textbf{Equation 1.3}$$

where λ_r is the resonant wavelength, r is the radius of the resonator, n_{eff} is the effective refractive index of the resonant mode, and m is an integer number of wavelengths in a roundtrip inside the cavity. A strong exponentially decaying evanescent field is formed due to continuous TIR of light trapped inside the resonator, which extends into the surrounding medium a few hundred nanometers, and can interact and respond to external environment changes. According to **Eq. 1.3**, a linear relationship exists between the resonant wavelength (λ_r) and the effective refractive index (n_{eff}). Therefore, resonant wavelength shifts can be used to detect changes in the refractive index of the surrounding medium, which is an important principle for the use of WGM resonators as label-free refractometric and biological sensors.[3-5]

1.2.1 Light Coupling Methods and Measurement

Near field evanescent coupling has shown high efficiency to couple light into WGM

resonators by significantly overlapping the evanescent fields of the cavity and the coupler.[6] Prisms, side-polished fibers, and thinned fibers are common coupling materials used to excite WGMs, as shown in **Fig. 1.4**.

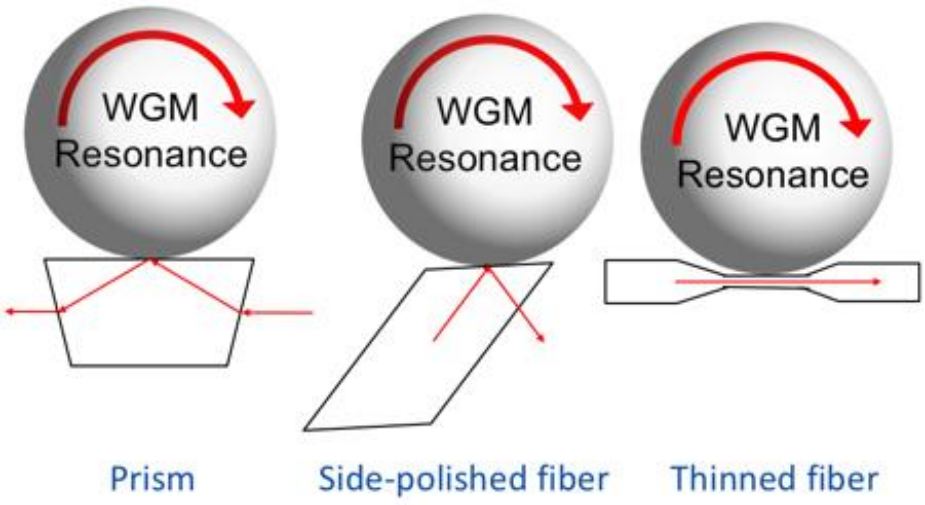

Figure 1.4. Light is near field evanescent coupled into WGM microcavities by using a prism, side-polished fiber and thinned fiber, respectively.

Among these methods, tapered fibers have been reported to achieve high coupling efficiency above 99%.[7] However, the small diameter of the tapered fiber (several micrometers) makes it mechanically fragile.[8] Additionally, if there is any change in the position of the fiber with respect to the resonator, the resonant wavelength will also change. This makes it difficult to accurately measure the refractive index changes from the surrounding medium or binding events.[9] In addition, the air-silica boundary is easily contaminated, which increases noise.[10]

In contrast, although prism coupling is reported to have a lower coupling efficiency (80%), it is more stable and easier to control.[11] Therefore, a Dove prism is utilized to couple light into the resonator in this work. **Figure 1.5** illustrates a simplified process for the WGM resonant wavelength measurement of a microsphere resonator. The light emitted from a tunable laser is

coupled into a Dove prism and captured inside the microsphere through TIR, while the evanescently scattered light is measured by an avalanche photodiode detector (APD). When the laser is tuned to the resonant wavelength, a characteristic Lorentzian peak can be observed in the plot of intensity versus wavelength, which is a manifestation that the electromagnetic energy is trapped within the cavity.[12]

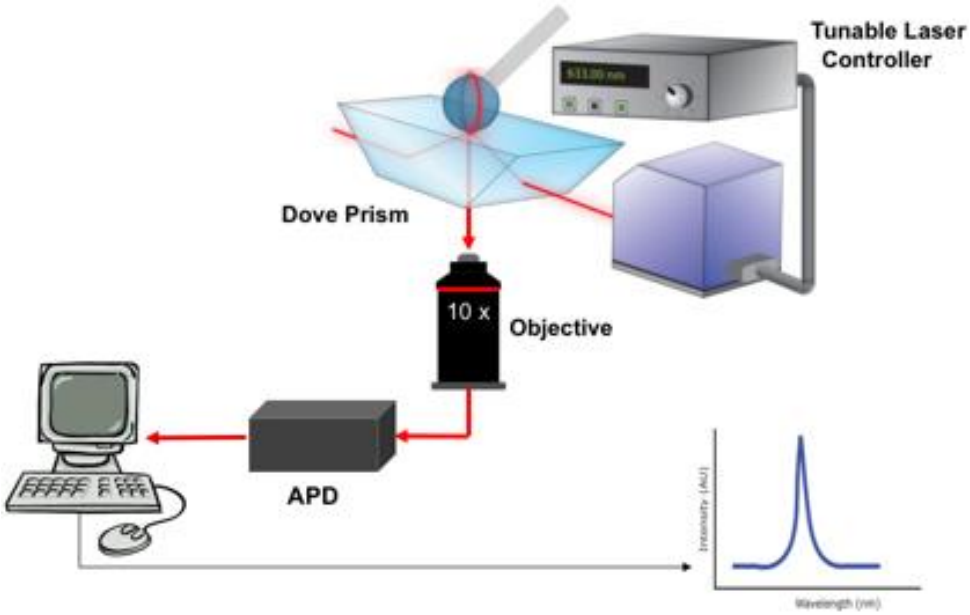

Figure 1.5. Schematics of the measurement for WGM resonant wavelength. Light from a tunable laser transferring to a dove prism is coupled into a silica microsphere via TIR. The evanescently scattered light is detected by an avalanche photodiode. The corresponding resonant wavelength is recorded showing a peak at wavelength-light intensity curve at the same time.

1.2.2 Whispering Gallery Mode Resonators for Biosensing

WGM resonators have been successfully used as sensors in the biomolecular sensing field. **Figure 1.6** illustrates the operation theory of WGM biosensors.[4] Analyte molecules (purple) covalently bind to the immobilized antibodies (blue) on the resonator surface. Since the refractive index of most biomolecules ($n =\sim 1.5$) is greater than that of the surrounding buffer

solution ($n =\sim 1.33$),[4] the binding event of biomolecules on the resonator surface increases the effective refractive index (n_{eff}), which leads to a quantitative red shift of the resonant wavelength. Therefore, the WGM resonant wavelength shift can be used to detect biomolecules. The magnitude of the resonant wavelength shift is illustrated in **Eq. 1.4**:[3]

$$\frac{\Delta\lambda}{\lambda} = \alpha_{ex}\frac{\sigma}{\varepsilon_0(n_s^2-n_m^2)R_0} \qquad \textbf{Equation 1.4}$$

where σ represents the surface coverage of analyte molecules, n_s and n_m are refractive indexes of the cavity material and the surrounding medium, respectively. α_{ex} is the excess polarizability and R_0 is the resonator radius. A biomolecule binding event can cause a change in the excess polarizability, which is proportional to the molecular weight. Thus, the amount of target molecules in solution can be quantitatively determined by measuring shifts in the WGM resonance, as illustrated in **Fig.1.6**.

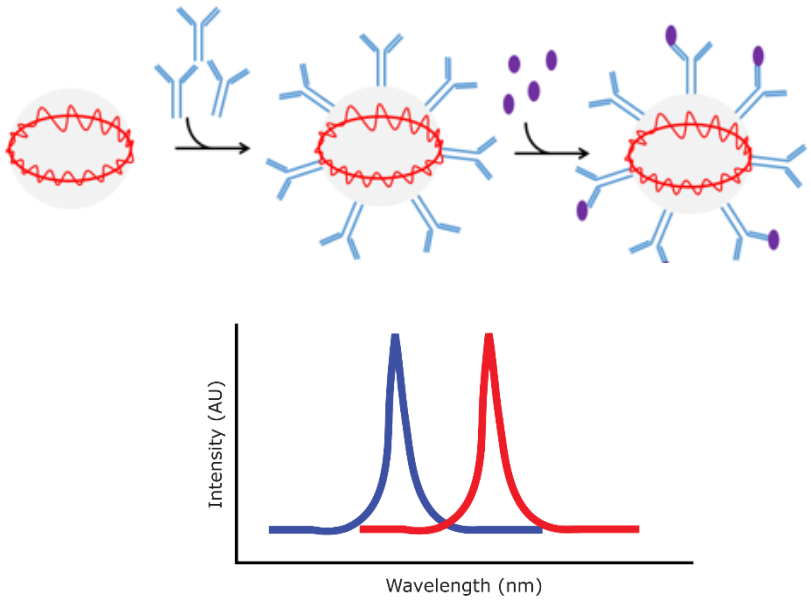

Figure 1.6. Schematics of the biosensing method using a WGM resonator. When analytes bind to the antibodies on the resonator surface, a red-shift of the resonant wavelength is observed. The amount of bound analytes can be quantified by analyzing the magnitude of the resonant wavelength shift.

1.3 Resonator Performance Metrics

In order to optimize sensing performance, some important parameters are necessary to consider. These performance metrics are discussed in the following section, including quality factor (Q-factor), photon lifetime, effective path length, free spectral range, mode volume, and finesse.

1.3.1 Quality Factor and Loss Mechanism

The Q-factor is an important parameter to characterize a resonator's performance, which is proportional to the time that light is coupled inside the resonator.[8] Q-factor can be used to measure the storage capacity of a resonator. The ratio of the resonant wavelength to linewidth is a common method to determine the Q-factor, as expressed in **Eq. 1.5:**

$$\boldsymbol{Q = \frac{\lambda_r}{\delta\lambda_r}} \qquad \textbf{Equation 1.5}$$

where λ_r is the resonant wavelength, and $\delta\lambda_r$ is the linewidth (full width half maximum, FWHM) of the resonant peak. Both can be obtained by the Lorentzian fitting. The higher Q-factor, the more efficient that light is captured and recirculated within the resonator. For sensing applications, a high Q-factor is desirable. As the Q-factor increases, the resonance linewidth decreases, which enables the measurement of smaller resonant wavelength shifts.[13] Meanwhile, the Q-factor is directly associated with the number of revolution light makes within the resonator, therefore, high Q-factor is beneficial to enhance the light-matter interaction length. It has been reported that Q-factor of microsphere resonators could reach as high as 8×10^9 at 633 nm.[14] The Q-factor is limited by the loss mechanisms which explains the main factors causing light to leak out of a resonator. Therefore, it is necessary to understand the loss mechanism to achieve a high Q-factor. For microsphere resonators, the total light loss consists of both intrinsic

and external losses. The external loss derives from the coupling method. The intrinsic loss is related to the resonator size, material and surface conditions, as shown in **Eq. 1.6**:[15]

$$\boldsymbol{Q^{-1} = Q_{rad}^{-1} + Q_{mat}^{-1} + Q_{s.s}^{-1} + Q_{cont}^{-1}} \qquad \textbf{Equation 1.6}$$

where Q_{rad} is radiation loss or bending loss, it is highly dependent on the size of a resonator. Some of the light leaks out of the cavity since the TIR at a curvature surface is never complete. As the resonator radius increases, radiation loss decreases due to small curvature angles.[15,16] At excitation wavelength of 633 nm, when the diameter of a microsphere resonator is equal to or larger than 30 μm, this radiation loss is minimal.[17] In addition to the resonator radius, light loss is also associated with material absorption (Q_{mat}). The most important source of material loss often comes from the light absorption by the cavity material or the surrounding medium.

Equation. 1.7 can be used to estimate the material loss by using an absorption decay constant α_m:[17,18]

$$\boldsymbol{Q_m = \frac{2\pi n_1}{\lambda \alpha_m}} \qquad \textbf{Equation 1.7}$$

where n_1 is the refractive index (~1.457 at 633 nm) of silica resonator, λ is the resonant wavelength. The absorption decay constant α_m is related to factors such as how tightly the light is confined within a resonator, the wavelength range, and the measurement environment. For WGM optical resonators operated in aqueous environment, their Q_m is usually higher when using lasers of the visible spectrum instead of the near-infrared range, because water has a larger α_m in the near-infrared spectra. $Q_{\text{s.s}}$ refers to scattering loss, which originates from surface roughness and contamination. The microsphere fabrication process may also decrease Q-factor via surface contaminants (Q_{cont}). By improving the fabrication technique to make the surface smoother and less contaminated, losses associated with scattering and contamination can be reduced.

1.3.2 Effective Path Length

The effective path length (L_{eff}) describes the length of light-analyte interactions within a cavity, which is linearly proportional to the Q-factor, as illustrated in **Eq. 1.8:**[14]

$$L_{eff} = \frac{Q\lambda_r}{2\pi n} \qquad \textbf{Equation 1.8}$$

here Q describes the Q-factor, λ_r is the resonant wavelength, and n is the refractive index of the cavity. L_{eff} for WGM optical resonators is determined by the number of times the light circulates within the microsphere, not by the cavity radius.[5] Photons in a resonator may circulate hundreds to thousands of times on average. Therefore, the effective path length can be as long as tens to hundreds of centimeters, rather than the resonator size which is micrometers.[13]

1.3.3 Free Spectral Range

The free spectral range (FSR), illustrated in **Fig. 1.7**, is the wavelength difference between two adjacent modes in a resonator and is determined by the excitation wavelength and the cavity size, which can be estimated by using **Eq. 1.9**:[19]

$$\Delta\lambda_{FSR} \approx \frac{\lambda^2}{2\pi nR} \qquad \textbf{Equation 1.9}$$

where λ is the resonant wavelength, R is the cavity radius, and n is the refractive index of the resonator. According to this equation, decreasing the radius of the resonator should provide a larger FSR, which is beneficial for distinguishing two adjacent modes.

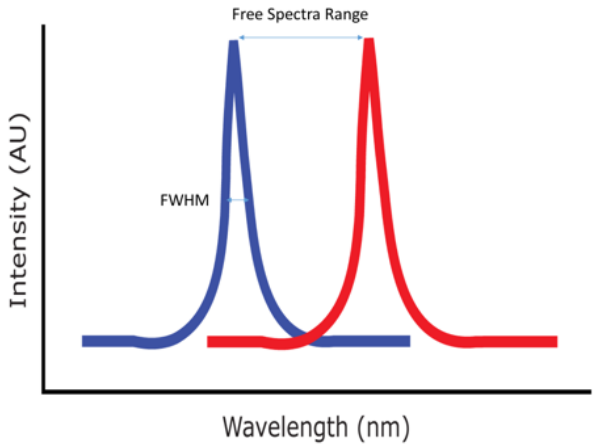

Figure 1.7. The free spectral range and full width at half maximum (FWHM, linewidth) of a cavity.

1.3.4 Mode Volume

The mode volume (V) of an optical resonator is described as the equivalent volume that the WGM occupies.[12] The WGM resonator' mode volume has great influence on the electromagnetic field strength at its surface.[4] **Figure 1.8** shows two different mode volumes. The electric field distributes widely when the mode volume is large (**Fig. 1.8. A**). On the contrary, the electric field is more concentrated at the sensing surface for a smaller mode volume (**Fig. 1.8. B**). Therefore, a small mode volume is favorable to achieve a large electromagnetic field strength, which is advantageous for sensing applications.[17,20] Additionally, the excitation wavelength can affect the mode volume. A smaller mode volume can be achieved by using shorter excitation wavelength sources. Hence, in this work, to optimize the sensor's performance, we select a short wavelength of 633 nm instead of the near-infrared wavelengths used elsewhere.

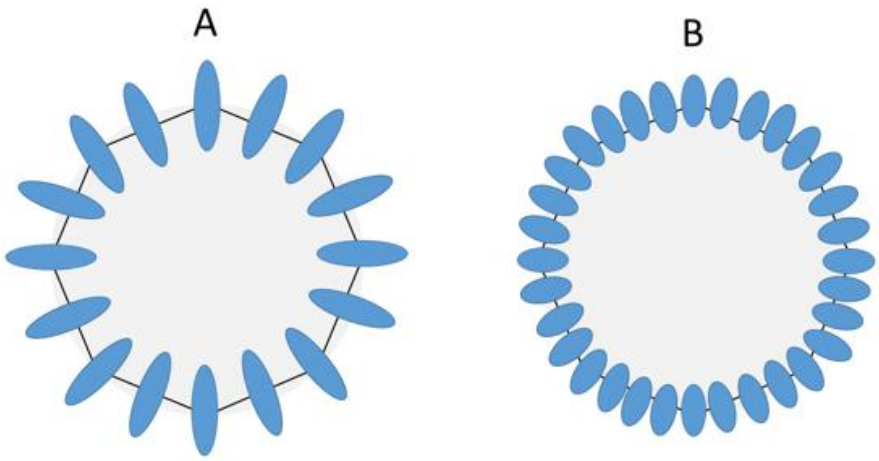

Figure 1.8. Images A and B illustrate large and small mode volume for a WGM microsphere resonator, respectively. Small mode volumes have more concentrated electric field, which are more desirable for surface sensing applications.

1.3.5 Finesse

Finesse (F) is another important parameter that can be used to characterize the performance of WGM resonators. The definition of finesse is the ratio of the free spectral range to the FWHM linewidth. Therefore, large finesse means the resonant peaks are narrow, which is usually desirable to obtain more accurate sensing results. Finesse is also related to the Q-factor and mode volume. **Equation. 1.10** shows the relationship:[18]

$$\boldsymbol{F \propto \frac{Q}{V}} \qquad \textbf{Equation 1.10}$$

because of this relationship, microcavities with large Q-factor and small mode volume are desired for sensing applications.

WGM resonators have many advantages for sensing purposes and much work has been done in the last 20 years to optimize this platform. The geometries, materials and sensing performance of WGM resonator have thus been investigated.

1.4 WGM Resonator Geometries and Comparison

A variety of dielectric materials can be used to fabricate WGM resonators, including silica, silicon, polymers and liquid droplets.[4] **Figure 1.9** shows several common microscale resonator geometries, including capillarys, toroids, rings, and spheres that have been reported to support WGM resonances. They are used for the detection of various biomolecules including proteins, viruses, and DNA.[15] Each geometry has their unique advantages and limitations, which are briefly listed in Table 1.1. More details are further discussed below.

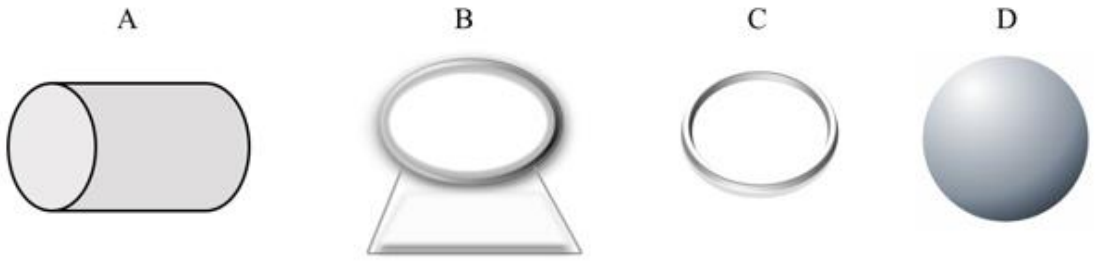

Figure 1.9. A variety of spherical resonator geometries support WGM resonances, including liquid core optical ring (A), microtoroid (B), microring (C), microsphere (D).

Table 1.1. WGM geometries and biosensing performance comparison

Optical Resonator Geometry	**Detection Limits**	**Quality Factors**	**Refractive Index Sensitivity (nm/RIU)**	**Advantages and Limitations**
Liquid Core Optical Ring Resonator (LCORR) [21,22]	10^{-4} – 10^{-7} RIU (Refractive Index Unit)	10^3-10^5	40	+ Fluidic handing capability + Low sample consumption - Dangerous and time consuming fabrication - Low Q-factors - Not robust - Hard to realize multiplex sensing
Microtoroid Resonator[23]	10^{-4}-10^{-6} RIU	$>10^8$	10	+ High Q-factors + Well controlled physical dimensions - Complex fabrication - Individual functionalization
Planer Ring Resonator[24,25,26]	10^{-4}-10^{-6} RIU	10^3-10^5	70-400	+ Mass fabrication + Easy to incorporate with chip technology + Multiplex detection + High RI sensitivity - Low Q-factors - Individual functionalization
Microsphere resonator[5,27,28]	10^{-7} RIU Single molecule	10^5-10^9	20-50	+ Low cost + Easy fabrication + High Q-factors - Hard to realize multiplex sensing - Not robust - Individual functionalization - Lack of mass production capability - Difficult to integrate with fluidics

1.4.1 Liquid Core Optical Ring Resonators (LCORR)

A liquid core optical ring resonator (LCORR) is a capillary-based ring resonator. The ring is formed in the circular cross section of a fused silica capillary, where the WGM resonance is excited. The capillary has an extremely thin wall of 3-5 μm, which allows the evanescent field to reach the capillary core and interact with analytes.[21] Light circulating repeatedly within the ring enhances the light-analyte interaction and improves detection limits. The geometry of LCORR makes it show excellent fluid handing capabilities, so it is compatible with capillary techniques to deliver fluid.[22] However, since HF etching is used to create the thin capillary walls, the fabrication process can be dangerous and time consuming. Meanwhile, the etching procedure creates large surface roughness, which limits the Q-factors. In addition, LCORRs are very fragile, which makes them difficult to integrate into a robust system. It is also difficult to perform multiplex sensing using this geometry.

1.4.2 Microtoroid Resonators

Microtoroid resonators are 3-D silica resonators that are fabricated on a silicon chip and have been demonstrated to obtain ultrahigh-Q factors ($> 10^8$).[23] The physical dimensions of a micro toroid resonator can be well controlled to accurately produce the desired size. However, the fabrication process is complex and elaborate, comprising of photolithography, pattern transfer into the silicon dioxide layer, dry etching and CO_2 laser selective reflow. Expensive equipment and long fabrication times are required to make microtoroid resonators. **Figure 1.10** illustrates the production procedures. In addition, precise alignment of an optical tapered fiber is needed to excite WGM of microtoroid resonators. Moreover, only individual functionalization can be realized for this 3-D geometry, which limits multiplex sensing.

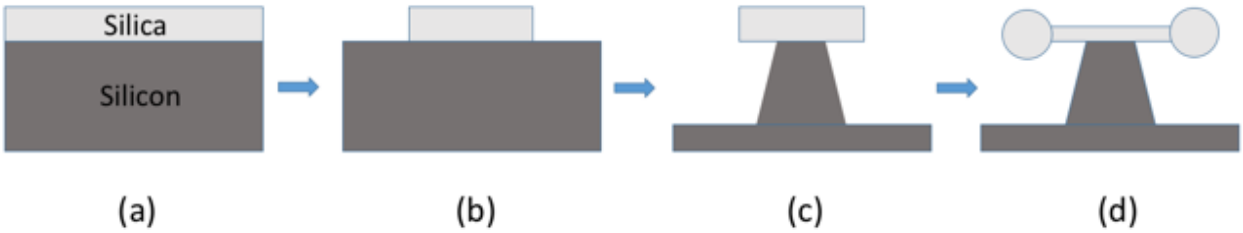

Figure 1.10. Fabrication procedures of silica microtoroids. (a) A photoresist layer is deposited on a Silica-Silicon wafer by photolithography. (b) HF wet etching creates silica pads. (c) Silica microdisks are isolated from the silicon substrate via a high-selectivity XeF_2 dry etching. (d) CO_2 laser reflow produces microtoroid resonators.

1.4.3 Planar Ring Resonators

Planar ring resonators are normally small waveguides that can be fabricated onto a solid substrate, such as silicon or silicon nitride using mature photolithography techniques.[24] Thanks to the well developed microfabrication technologies, mass fabrication can be realized to manufacture planar ring resonators to exact specific requirements. Moreover, this type of resonator can be fabricated onto a chip to achieve excellent fluid handing capabilities, which is advantageous in clinical applications.

Additionally, planar ring resonators have been demonstrated to enable multiplexed detection, and to achieve high sensitivity (70-400 nm/RIU).[25,26] However, the Q factors for this type of resonators are usually small (10^3-10^4) and individual functionalization of the resonators can be tedius.

1.4.4 Microspheres Resonators

Microspheres have some advantages over other geometries such as low costs, easy fabrication, and high Q-factors, making them good candidates for WGM sensing applications. Silica microspheres with smooth surface and accurately controlled size can be fabricated via

melting techniques. Melting the tip of an optical fiber is a convenient and inexpensive method to obtain a high quality single sphere with precise diameter in a range of 10-200 μm. Upon heating the tip of a single mode silica fiber that has had its jacket removed, a highly spherical and uniform bulb is formed through surface tension, which has small surface scattering loss. An oxygen/butane or nitrous oxide/butane microtorch, a high-power CO_2 laser or an electric fusion arc are commonly utilized to melt the fiber tip. Fused silica microspheres have shown ultrahigh Q-factors ranging from 10^8-10^9 due to their smooth surfaces.[4] Such high Q-factors can be used to study systems with low detection limit.[27,28] However, microsphere resonators also have several drawbacks. For example, it is challenging to integrate them with fluidics technology.[5]

1.5 Opportunities for Microsphere Whispering gallery mode resonators

Compared with other common geometries, microsphere resonators are advantageous candidates for assay development because they are easy to functionalize and inexpensive, commercially available and easily fabricated at desired sizes. In addition, the melting fabrication technique allows microspheres to obtain exquisitely smooth spherical surfaces, which reduces scattering loss leading to ultrahigh Q-factors. A large Q-factor implies that the resonator has a long effective path length and narrow resonance linewidth, which are highly desirable characteristics in sensing platforms. Therefore, in this thesis, fused silica microspheres are utilized for sensing applications. We systematically study how a microsphere's size and temperature affect its performance.

1.6 Overview of the thesis

Whispering gallery mode resonators are miniature optical devices which can provide sensitive label-free detection. Light is confined within resonators via total internal reflection, creating evanescent waves to sense the refractive index change of the surrounding medium or surface binding events. In order to optimize the performance of WGM microcavities, large Q-factors and high sensitivities are desirable.

Chapter 2 discusses the resonator size effects on silica microspheres' Q-factor and bulk solution sensitivity. Meanwhile, temperature influence is also studied. Silica microspheres of 45μm in diameter achieve large Q-factor in air and high sensitivity with the smallest thermal impact and are selected for sensing.

Chapter 3 studies the application of silica microsphere resonators in biosensing. DOPC/GM1 bilayers which are uniformly transferred onto resonators via the Langmuir-Blodgett technique can be used to detect the binding of cholera toxin molecules to GM1 molecules. The binding event is monitored via the observation of whispering gallery mode resonant wavelength shifts. Langmuir-Blodgett films provide an easy approach for systematically changing the density of receptors and quantify in their effect on resonator sensitivity.

1.7 References

1. Ahuja, D.; Parande, D., Optical sensors and their applications. *J. Sci. Res. Rev.* **2012,** *1* (5), 60-68.
2. Vollmer, F.; Arnold, S., Whispering-gallery-mode biosensing: label-free detection down to single molecules. *Nat. Methods* **2008,** *5* (7), 591-596.
3. Lin, C. A.; Chen, J. H.; Wang, L. A., High-Q Si Microsphere Resonators Fabricated From Si-Cored Fibers for WGMs Excitation. *IEEE Photonics Technology Letters* **2015**, 27 (13), 1355-1358.
4. Ward, J.; Benson, O., WGM microresonators: sensing, lasing and fundamental optics with microspheres. *Laser Photonics Rev.* **2011,** *5* (4), 553-570.
5. Fan, X.; White, I. M.; Shopova, S. I.; Zhu, H.; Suter, J. D.; Sun, Y., Sensitive optical biosensors for unlabeled targets: A review. *Anal. Chim. Acta* **2008,** *620* (1-2), 8-26.
6. Gorodetsky, M. L.; Ilchenko, V. S., Optical microsphere resonators: optimal coupling to high-Q whispering-gallery modes. *J. Opt. Soc. Am. B* **1999,** *16* (1), 147-154.
7. Cai, M.; Painter, O.; Vahala, K. J., Observation of Critical Coupling in a Fiber Taper to a Silica-Microsphere Whispering-Gallery Mode System. *Phys. Rev. Lett.* **2000,** *85* (1), 74-77.
8. Laine, J.-P. J. V. Design and applications of optical microsphere resonators. **2003**.
9. Guo, Z.; Quan, H.; Pau, S., Near-field gap effects on small microcavity whispering-gallery mode resonators. *J. Phys. D: Appl. Phys.* **2006,** *39* (24), 5133-5136.
10. Hendrickson, S. M.; Pittman, T. B.; Franson, J. D., Nonlinear transmission through a tapered fiber in rubidium vapor. *J. Opt. Soc. Am. B* **2009,** *26* (2), 267-271.
11. Sarid, D., High efficiency input-output prism waveguide coupler: an analysis. *Appl Opt* **1979,** *18* (17), 2921-6.

12. Matsko, A. B.; Ilchenko, V. S., Optical resonators with whispering-gallery modes-part I: basics. *IEEE J. Sel. Top. Quantum Electron.* **2006,** *12* (1), 3-14.

13. Luchansky, M. S.; Bailey, R. C., High-Q Optical Sensors for Chemical and Biological Analysis. *Anal. Chem. (Washington, DC, U. S.)* **2012,** *84* (2), 793-821.

14. Gorodetsky, M. L.; Savchenkov, A. A.; Ilchenko, V. S., Ultimate Q of optical microsphere resonators. *Opt. Lett.* **1996,** *21* (7), 453-455.

15. Chiasera, A.; Dumeige, Y.; Feron, P.; Ferrari, M.; Jestin, Y.; Conti, G. N.; Pelli, S.; Soria, S.; Righini, G. C., Spherical whispering-gallery-mode microresonators. *Laser Photonics Rev.* **2010,** *4* (3), 457-482.

16. Quan, H.; Guo, Z., Analyses of Whispering-Gallery Modes in Small Resonators. *Journal of Micro/Nanolithography, MEMS and MOEMS* **2009,** *8* (3), 033060-7.

17. Gorodetsky, M. L.; Pryamikov, A. D.; Ilchenko, V. S., Rayleigh scattering in high-Q microspheres. *J. Opt. Soc. Am. B* **2000,** *17* (6), 1051-1057.

18. Kippenberg, T. J. A. Nonlinear optics in ultra-high-Q whispering-gallery optical microcavities. 2004.

19. Gamba, J. M. Whispering gallery mode resonators as biosensors.

20. Yoshie, T.; Tang, L.; Su, S.-Y., Optical microcavity: sensing down to single molecules and atoms. *Sensors (Basel)* **2011**, 11 (2), 1972-91.

21. Zhu, H.; White, I. M.; Suter, J. D.; Dale, P. S.; Fan, X., Analysis of biomolecule detection with optofluidic ring resonator sensors. *Opt. Express* **2007**, 15 (15), 9139-9146.

22. Suter, J. D.; White, I. M.; Zhu, H.; Fan, X., Thermal characterization of liquid core optical ring resonator sensors. *Appl Opt* **2007**, 46 (3), 389-96.

23. Armani, D. K.; Kippenberg, T. J.; Spillane, S. M.; Vahala, K. J., Ultra-high-Q toroid microcavity on a chip. *Nature (London, U. K.)* **2003**, 421 (6926), 925-928.

24. Zhu, H.; Suter, J. D.; Fan, X., Label-free optical ring resonator bio/chemical sensors. *Springer Ser. Chem. Sens. Biosens.* **2010**, 8 (Optical Guided-Wave Chemical and Biosensors II), 259-279.

25. Washburn, A. L.; Luchansky, M. S.; McClellan, M. S.; Bailey, R. C., Label-free, multiplexed biomolecular analysis using arrays of silicon photonic microring resonators. *Procedia Eng.* **2011**, 25, 63-66.

26. Washburn, A. L.; Luchansky, M. S.; Bowman, A. L.; Bailey, R. C., Quantitative, Label-Free Detection of Five Protein Biomarkers Using Multiplexed Arrays of Silicon Photonic Microring Resonators. *Anal. Chem. (Washington, DC, U. S.)* **2010**, 82 (1), 69-72.

27. Armani, A. M., et al., Label-Free, Single-Molecule Detection with Optical Microcavities. *Science*. **2007**, 317 (5839), 783-787.

28. Vollmer, F.; Braun, D.; Libchaber, A.; Khoshsima, M.; Teraoka, I.; Arnold, S., Protein detection by optical shift of a resonant microcavity. *Appl. Phys. Lett.* **2002**, 80 (21), 4057-4059.

Chapter 2

Studying the Cavity Size and Temperature Effects on the Performance of WGM Resonators

2.1 Introduction:

In recent decades, optical silica microsphere resonators have become attractive sensors due to their various advantages, such as low cost, easy fabrication, and high Q-factor. The whispering gallery mode (WGM) resonances are highly related to the resonator's morphology. Therefore, they are also called optical-morphology-dependent resonances (MDRs). In this chapter, we discuss how the size of silica microsphere resonators influences their WGM performance in details. Since thermal noise is usually the main noise in WGM study, we also research the temperature fluctuation effects on the WGM resonances. For sensing applications, WGM resonators with larger Q-factor and high sensitivity are desirable. Therefore, our interest is to find the optimal size of silica microspheres for research.

2.2 WGM Resonator Sensing Principles

Before studying what affects the performance of WGM resonators, their sensing principle needs to be understood first. As discussed in the chapter 1, it is known that light is coupled into WGM resonators via total internal reflection (TIR). When the optical path length within a cavity is an integer number of incident wavelength, constructive interference occurs, leading to the WGM resonance. The resonant wavelength λ_r depends on the resonator radius r and its effective

refractive index n_{eff} ($\boldsymbol{\lambda_r = \frac{2\pi r n_{eff}}{m}}$). The resonant wavelength change can be expressed as **Eq. 2.1**:[1]

$$\frac{d\lambda_r}{\lambda_r} = \frac{dr}{r} + \frac{dn_{eff}}{n_{eff}} \qquad \textbf{Equation 2.1}$$

where $d\lambda_r$, dr and dn_{eff} are the changes of resonant wavelength, cavity radius and effective refractive index of the optical mode, respectively. Therefore, a small variation in the cavity size can alter the resonant wavelength significantly. Meanwhile, TIR within resonators creates an evanescent field, which has a length of tens to several hundreds of nanometers. It exponentially decays and penetrates into the surrounding medium, resulting in the interaction between the light and the analyte. **Figure 2.1** illustrates this phenomenon. Either the change in refractive index of the surrounding medium or the binding or removal of molecules events at the resonator surface will change the n_{eff}, leading to a resonant wavelength shift.[2] Consequently, WGM resonators can be used to analyze bulk medium refractive index change and to quantitative detect biomolecules as well.[3]

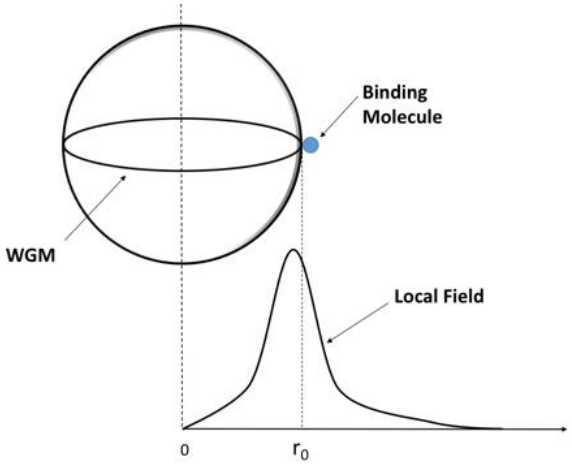

Figure 2.1 The evanescent field of the WGM penetrates into the surrounding medium and interacts with the nearby molecules, a binding molecule on the microsphere's interface can be detected.

2.3 Fabrication of Silica Microspheres

A single silica microsphere can be fabricated by melting the tip of an optical glass fiber via surface tension. This method is not expensive and allows for forming spheres with well controlled diameter and smooth surface, which largely reduces scattering loss. In this research, S630-HP fused silica fiber, a high performance single mode fiber with a core diameter about 3.5 μm and cladding diameter about 125 μm was utilized as the resonator material. The fiber was first stripped to remove the plastic jacket and cleaned with alcohol, then a high power heat source (ARC Fusion Splicer, FSM-40S, Fujikura) was used to melt the fiber tip. ARC Fusion Splicer is a mechanic-thermal machine which is originally used to align two optical fibers and fuse them together via an electric arc. For our purpose, it was utilized to heat a fiber to form a microsphere. The fiber was placed ~2 mm away from the electrodes and heated by manually arcing. For fabricating small spheres (diameters in the range of 10 μm-110 μm), a tapered fiber was made first. A tapered optic fiber with long, and thin sub-micron tip was formed through a heating and pulling technique with a P-2000 micropipette puller (Sutter instruments) via the following settings: heat 320, velocity 5, delay 0, and pull 100. Then the ARC splicer melted the tapered fiber to form a sphere. The size of microspheres was controlled by the position of the fiber and arc number, the minimum diameter we obtained was about 15 μm. **Figure 2.2** shows images of a tapered fiber and several fused silica microspheres with various diameters.

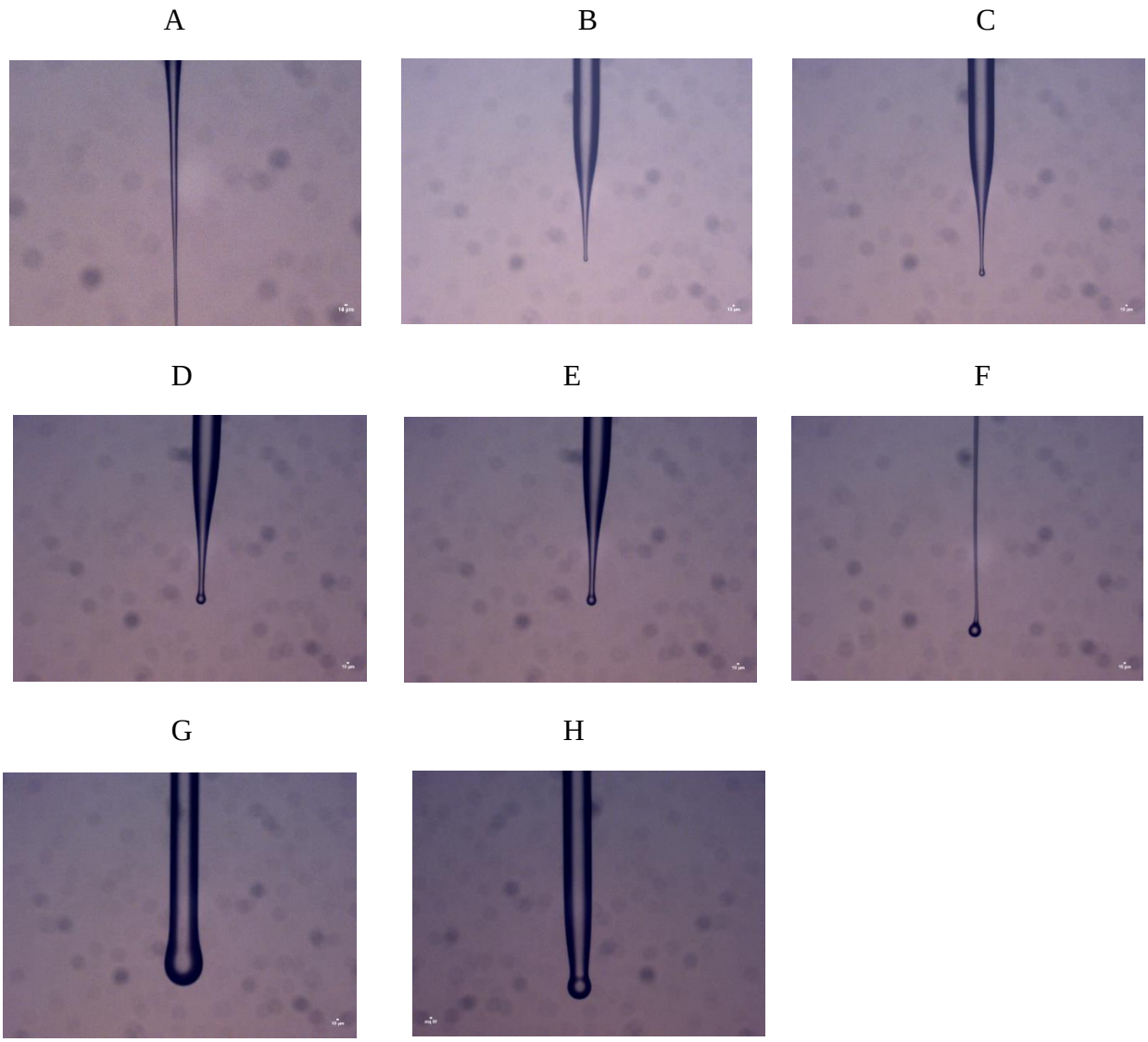

Figure 2.2. (A) A thin tapered fiber. (B-G) A variety of fused silica microspheres with different diameters (A-G are 15 µm, 23 µm, 33 µm, 45 µm, 56 µm, 104 µm, 163 µm in diameter, separately).

2.4 Whispering Gallery Mode Experimental Setup:

A common configuration of the WGM experimental setup for microsphere excitation and characterization is illustrated in **Fig. 2.3 (A)**. The excitation light emitted from a tunable diode laser (633 nm, Vortex 6000) was coupled into the fused silica microsphere via TIR through a Dove prism. A triangle voltage waveform was used to repeatedly scan the wavelength range of

approximately 300 pm with a scanning rate of 0.5 Hz. The evanescently scattered light from the resonator was viewed through an optical microscope (Nikon DIAPHOT 200) equipped with a 10x objective (Olympus, 0.3 NA) and detected by an avalanche photodiode detector (APD) (SPCM-AQR-14). A computer controlled the laser scanning and recorded the scattered signal. The scattered light intensity as a function of voltage was recorded and converted to wavelength to generate a WGM spectrum, as illustrated in **Fig. 2.3 (B).**

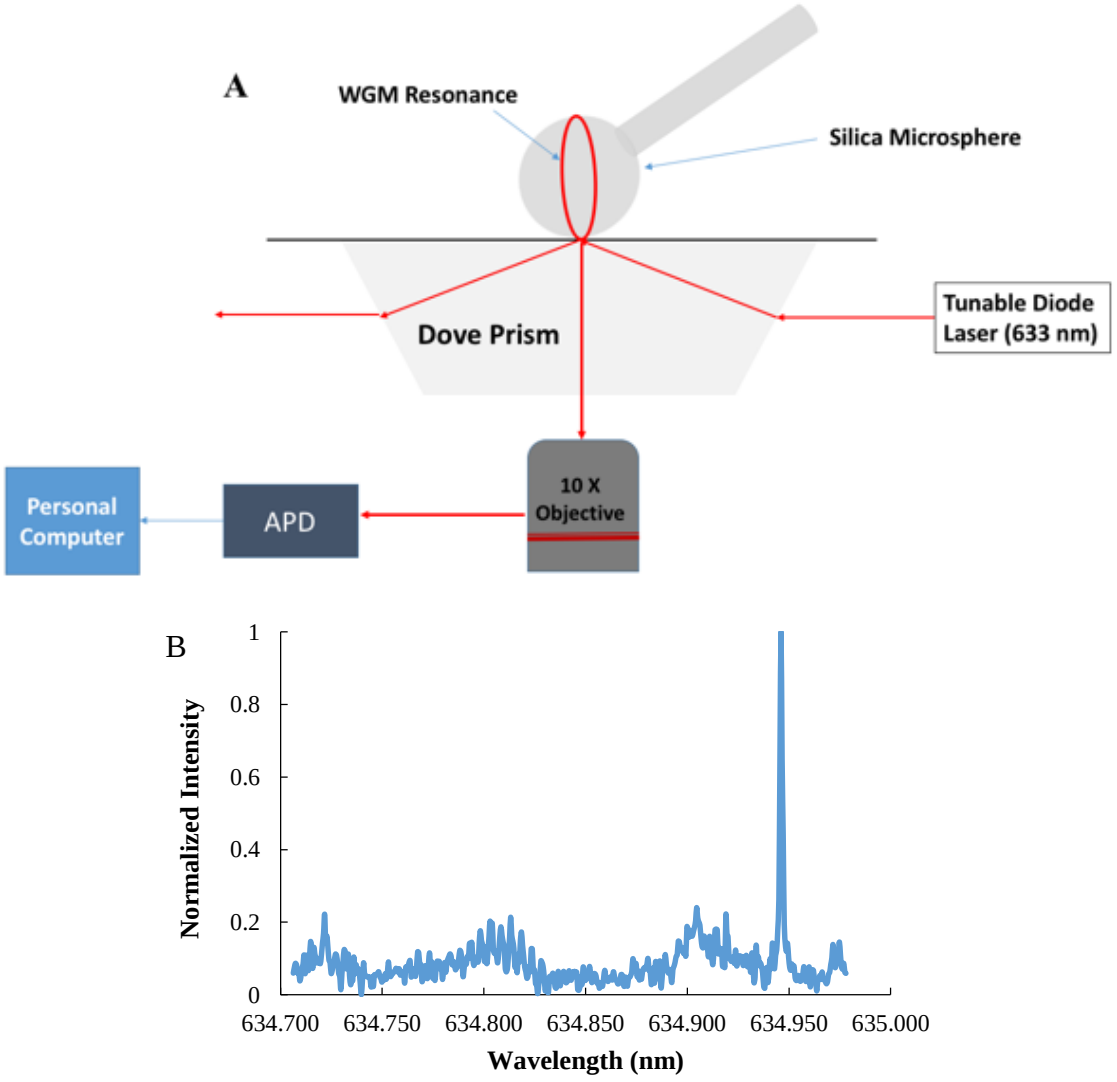

Figure. 2.3. (A) WGM experimental setup; (B) A resonant peak of a fused silica microsphere in the air.

2.5 Measurements of the Microsphere Performance

As mentioned, Q-factor and refractive index sensitivity are two important properties to measure the performance of a WGM resonator. Therefore, these two characteristics were analyzed in this thesis. Fused silica microspheres with various diameters were fabricated via surface tension, then the fiber stem of a silica microsphere was clamped stably on a XYZ stage and slowly brought in contact with the surface of a coverslip placed above the Dove prism. When light was coupled within the resonator, a resonance peak was observed. A Lorentzian curve fit was used to find the resonant wavelength and its corresponding linewidth. Q-factor was obtained by calculating the ratio of the resonant wavelength versus linewidth. Q-factors of microspheres were measured in air first. Bulk solution refractive index assays were then performed to calibrate the response of individual microspheres. A microsphere was slowly immersed in de-ionized (DI) water first, then NaCl stock solutions with various concentrations were injected to uniformly alter the refractive index of the medium. Upon the injection, the resonant wavelength shifts were observed in response to the homogeneous refractive index change.

2.6 Results and Discussion of Microsphere Size Effects on the Performance of Fiber Resonators

2.6.1 Q-factors of Silica Microspheres in Air and in Liquid

The Q-factors of silica microspheres with different diameters were analyzed in air and in liquid separately, results were listed in **Table 2.1**.

Table 2.1. Q-factors of silica microspheres with various diameters in air and in liquid.
(N=3, All the values below are average results)

Microsphere Diameter (μm)	Q-factor in Air	Q-factor in NaCl Solution
15 ± 2	$(2.6 \pm 0.3) \times 10^5$	N/A
23 ± 3	$(5.4 \pm 0.4) \times 10^5$	N/A
33 ± 2	$(9.4 \pm 0.3) \times 10^5$	$(0.9 \pm 0.2) \times 10^4$
46 ± 2	$(19 \pm 0.8) \times 10^5$	$(1.3 \pm 0.2) \times 10^4$
56 ± 3	$(1.6 \pm 0.3) \times 10^5$	$(3.5 \pm 0.3) \times 10^4$
104 ± 4	$(2.2 \pm 0.2) \times 10^5$	$(4.6 \pm 0.4) \times 10^4$
163 ± 3	$(6.1 \pm 0.1) \times 10^5$	$(84.5 \pm 0.4) \times 10^4$

In air, the Q-factor for microspheres initially increased with the increasing resonator diameter, then the value suddenly dropped, subsequently this parameter increased again as the diameter expanded. **Figure 2.4 (A)** depicts this phenomenon. The optimal diameter to obtain a high Q-factor in air was about 46 μm, which had a Q-factor of $\sim 1.9 \times 10^6$. On the other hand, it was found that the Q-factors significantly decreased in liquid versus air.[4] And larger microspheres had larger Q-factors, as shown in **Fig. 2.4 (B).**

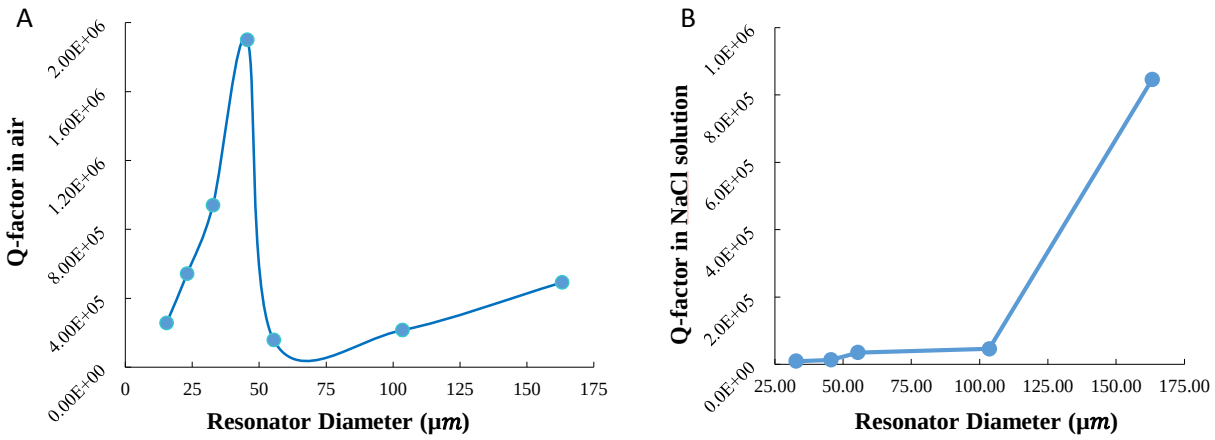

Figure 2.4. Q-factors comparison of microspheres with different diameters in air and in liquid.

As indicated in chapter 1, the Q-factor is a very important parameter, which describes the light coupling efficiency within a resonator. Since it can be expressed by the ratio between the resonant wavelength and linewidth, when the Q-factor increases, the linewidth decreases and the resonance peak is narrower, making it easier to measure a smaller wavelength shift.[5] Moreover, the effective length L_{eff}, characterizing the length of light-analyte interactions within the cavity, which illustrates the number of revolutions of the light supported by the resonator, increases with the increasing Q-factor ($L_{eff} = \frac{Q\lambda}{2\pi n}$). As the WGM resonance circulates repeatedly around the sphere surface, this light circulation significantly enhances the light interaction with analytes on the resonator surface.[2] The higher degree of light confinement results in longer effective path length and stronger resonator-analyte interaction, which is helpful to obtain a higher sensitivity.[6] Therefore, a large Q-factor is desirable. In order to increase the Q-factor, the light loss needs to be reduced. The total light loss consists of intrinsic loss and external loss. The external loss comes from the coupling method. In our work, a Dove prism is used to couple light. Thus, accurate phase matching between the microsphere and the prism is necessary to reduce the external loss. For the intrinsic loss, it is comprised of radiation loss, material loss, scattering loss and surface contamination loss, which greatly depends on the resonator size.

For fused silica microspheres, since they are fabricated by surface tension, ultra-smooth surfaces can be obtained, which largely reduces the surface roughness and contamination. Therefore, scattering loss and surface contamination loss are not regarded as the main limiting factors in determining the Q-factor in air. In addition, some of the light leaks out of a resonator since the TIR at a curved surface is never complete, which corresponds to the radiation loss. When the diameter of a microsphere is very small, the effective path length inside is also small, and light approaches the resonator interface in a steep angle, largely reducing the efficiency of

TIR. Therefore, within a certain diameter range, smaller microspheres have smaller Q-factors in air. With increasing the resonator size, radiation loss decreases, so Q-factor increases, which corresponds to the trend seen in **Fig. 2.4 (A)**. It appears that for microspheres with diameters larger than 30 μm, radiation loss is a minor factor.[7] Instead, as the size of microspheres increases, material loss arising from light absorption by both the resonator and surrounding medium becomes the primary limiting reason for Q-factor. In air, the Q-factor of the 56 μm diameter resonators suddenly dropped, which may be due to large material loss caused by water moisture adsorption onto microspheres. However, Q-factors of silica microspheres in liquid were significantly smaller than those in air. **Figure 2.5** shows an example of resonant spectra of a 45 μm diameter microsphere in air ($Q = 1.5 \times 10^6$) and in liquid ($Q = 1.2 \times 10^4$), where the peak in liquid is much broader than in liquid, which is likely a result of the increased scattering loss and large material loss by water absorption in liquid.[8]

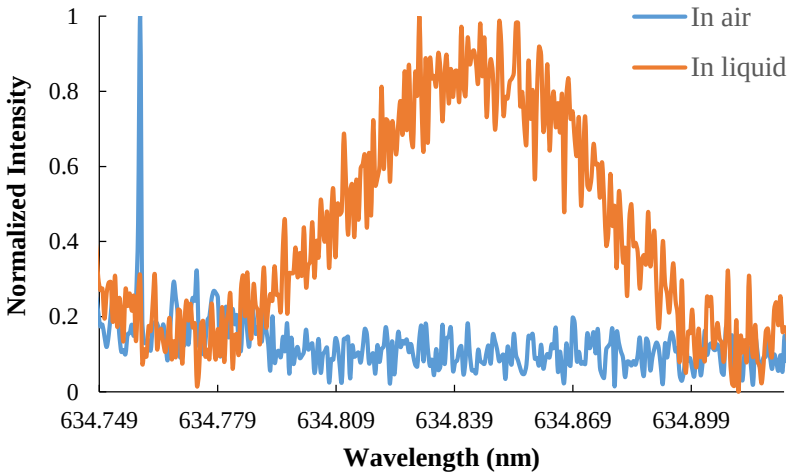

Figure 2.5. Resonant wavelength spectra of a single silica microsphere in air (blue) and in liquid (orange). The Q-facter in air ($Q = 1.5 \times 10^6$) is significantly higher than that in liquid ($Q = 1.2 \times 10^4$).

In addition, refractive index difference between the microsphere material ($n\sim1.46$) and the liquid medium ($n\sim1.33$) is smaller than that of microsphere with air ($n\sim1.00$). The larger refractive index contrast can cause light to be more tightly confined within a resonator, leading to less loss and a higher Q-factor.[9] When microspheres were immersed in liquid, the Q-factors increased with growing diameters, as shown in **Table 2.1** and **Fig.2.4 (B)**. For microspheres with diameters smaller than 30 μm, no obvious resonance was observed, which might be due to a combination of large radiation loss and water absorption loss. As the size of resonators increases, radiation loss becomes lower and Q-factors increase. However, the mode density increases with larger resonators as well, causing the overlap of Lorentzian transmission between several different modes, which makes it challenging to track the shift of a single resonant peak.[10] In addition, microspheres with larger diameters have smaller free spectra range ($\Delta\boldsymbol{\lambda_{FSR}} \approx \frac{\boldsymbol{\lambda^2}}{\boldsymbol{2\pi nR}}$) , making it harder to distinguish two adjacent modes. **Figure 2.6** illustrates an example of the resonant spectra of a large resonator ($D\sim160\ \mu m$). The resonator has multiple resonant peaks in liquid. Therefore, it is difficult to monitor a single wavelength shift when the refractive index of its surrounding medium is changed. By shortening the scanning wavelength range, fewer resonance peaks show up, letting it be possible to track the shift of a single peak.

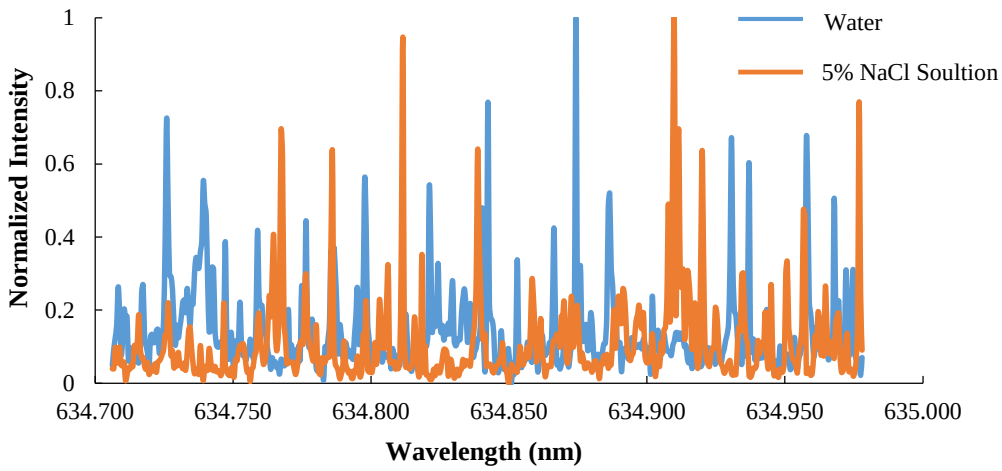

Figure 2.6. Resonant spectra of a resonator ($D \sim 160\ \mu m$) in water and their shift with adding NaCl solution to create a 5 mass% NaCl solution.

Continuing to increase the resonator's size results in a greater proportion of the WGM mode volume within the cavity itself instead of the surrounding medium. With regard to common biosensing applications, resonators with such large sizes are not as useful, hence we don't consider large diameter microspheres ($> 200\ \mu m$) in this work.[11]

2.6.2 Bulk Solution Refractive Index Sensitivity of Silica Microspheres

Sensor sensitivity is another significant parameter to evaluate in its performance. In general, sensitivity is the sensor's response to changes in analyte concentration. The sensitivity of optical sensors is dependent on the strength of the light-analyte interaction.[12-14] For WGM optical resonators, their refractive index sensitivity is defined as the magnitude in the resonant wavelength shift versus the change in refractive index of the sample, as shown in **Eq. 2.2**:

$$\boldsymbol{S = \frac{\Delta\lambda}{\Delta n}} \qquad \textbf{Equation 2.2}$$

where $\Delta\lambda$ and Δn represent the resonant wavelength shift and the refractive index change of the surrounding medium. In short, if the WGM wavelength is monitored for several different

refractive indexes, the sensitivity is the slope of the generated trend. The unit of sensitivity is nm/RIU, where RIU is the refractive index unit. In this work, in order to measure the sensitivity of resonators, a microsphere was immersed in water (n_2= 1.3325) first, then NaCl solution was slowly added to the water to uniformly increase the refractive index of the medium. Various refractive indexes of 5-6 spectra were recorded to calculate the sensitivity. **Figure 2.7** shows a resonator' resonant wavelength shifts versus the increasing solution refractive indexes (A), a corresponding linear (R^2= 0.9946) calibration curve (B) with a sensitivity of $\sim 50.4\ nm/RIU$ was obtained.

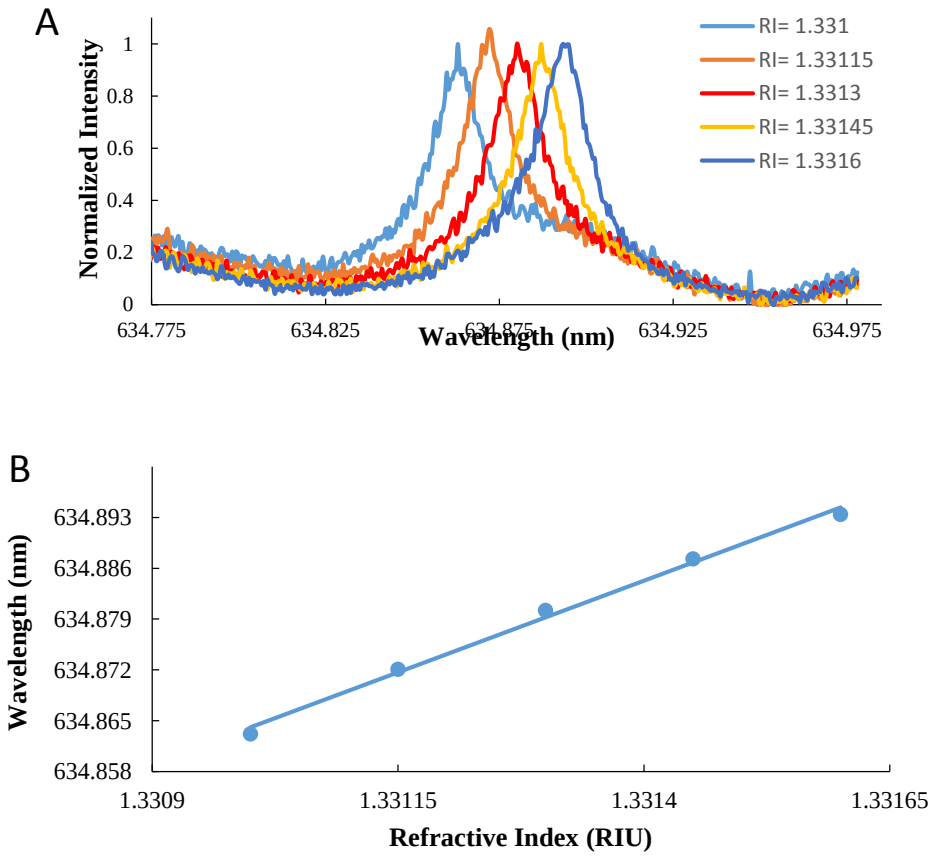

Figure 2.7. (A) Resonant wavelength shifts with the increasing solution refractive index. (B) The calibration curve showed a linear relationship (R^2= 0.9946) between the refractive index and the resonant wavelength. A measured sensitivity of the microsphere was $\sim 50.4\ nm/RIU$.

The size of a microsphere resonator not only affects its Q-factor, but also has a great influence on its sensitivity. Bulk solution refractive index sensitivities were measured for silica microspheres with different diameters. Results are shown in **Table 2.2**. **Figure.2.8** plotts the corresponding WGM resonant wavelength shifts versus refractive index changes for 5 microspheres with different diameters. These calibration curves all displayed excellent linearity.

Table 2.2. NaCl solution refractive index sensitivities of silica microsphere resonators with various diameters.
(N=3, all values below are average results)

Microsphere Diameter (μm)	***Sensitivity (nm/RIU)***
15 ± 2	N/A
23 ± 3	N/A
33 ± 2	14.5 ± 2.1
46 ± 2	56.5 ± 1.1
56 ± 3	26.7 ± 1.3
104 ± 4	21.0 ± 2.2
163 ± 3	36.7 ± 1.2

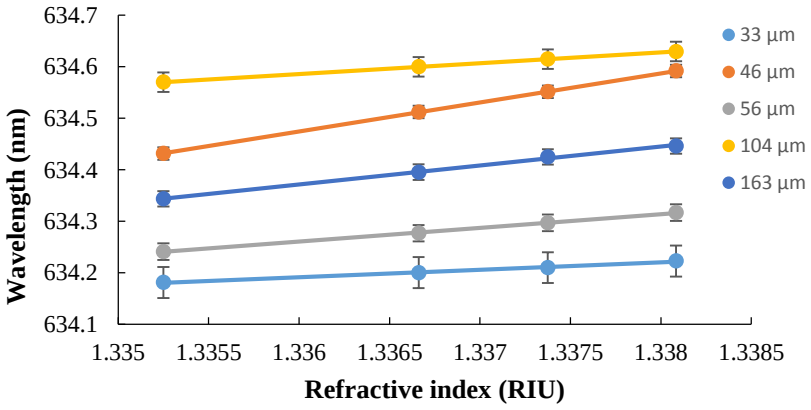

Figure. 2.8. Resonant wavelength shifts versus solution refractive index change of silica microspheres with different diameters. Perfect linearity was observed for all resonators.

According to **Table 2.2** and **Fig. 2.8**, the sensitivity was highly dependent on the microsphere size. For extremely small microspheres (D$\sim 15-35$ μm), their sensitivities were not observed or were quite low. Q-factors for these resonators were small in liquid due to large radiation loss, leading to short effective length L_{eff}. Thus, the light-medium interaction was not strong enough to provide high sensitivity. As the microsphere diameter (D$\sim 45-105$ μm) increased, higher sensitivity was obtained. In this diameter range, microspheres with small sizes had high sensitivities. This phenomenon was a result of a combination of several factors. First, larger Q-factors in bigger microspheres can support longer effective length and stronger resonator-analyte interaction, which is helpful for achieving high sensitivity. On the other hand, a more important factor that affects the sensitivity of a WGM microsphere is how tightly the light is coupled inside the sphere. For smaller microspheres it is easier for more photon energy to leak out, so their evanescent tails can extend further into the surrounding environment. This tremendously enhances the light-matter interaction, leading to higher sensitivity.[15] The length of the evanescent tail is inversely proportional to the resonator diameter; therefore, smaller microspheres are favorable. In order to better explain this phenomenon, theoretical mathematical analysis is as follows:

A microsphere of radius r with refractive index n_1 is immersed in a uniform surrounding medium with refractive index n_2. At resonance, the wave vector of the resonator is represented by k_0. Only considering the first-order whispering gallery mode, when n_2 is changed to $n_2 + \Delta n_2$, k_0 becomes to $k_0 + \Delta k$. The fractional shift $\frac{\Delta k}{k_0}$ of Transverse Electric (TE) and Transverse Magnetic (TM) modes can be calculated by **Eq.2.3** and **Eq.2.4**, respectively.[9]

$$\left(\frac{\Delta k}{k_0}\right)_{TE} \cong -\frac{n_2 \Delta n_2}{(n_1^2 - n_2^2)^{3/2}} \frac{1}{k_0 r} \qquad \textbf{Equation 2.3}$$

$$\left(\frac{\Delta k}{k_0}\right)_{TM} \cong -\frac{n_2 \Delta n_2}{(n_1{}^2 - n_2{}^2)^{3/2}}\left(2 - \frac{n_2{}^2}{n_1{}^2}\right)\frac{1}{k_0 r} \qquad \textbf{Equation 2.4}$$

Based on the fraction shift, sensitivity factors f_{TE} and f_{TM}, which are used to measure a resonator's sensing performance, can be obtained via **Eq.2.5** and **Eq.2.6**:

$$f_{TE} = -(\Delta k/k_0)_{TE}/[n_2 \Delta n_2 (n_1{}^2 - n_2{}^2)^{-1}] = \frac{1}{(n_1{}^2 - n_2{}^2)^{1/2}}\frac{1}{k_0 r} \qquad \textbf{Equation 2.5}$$

$$f_{TM} = -(\Delta k/k_0)_{TM}/[n_2 \Delta n_2 (n_1{}^2 - n_2{}^2)^{-1}] = \frac{1}{(n_1{}^2 - n_2{}^2)^{1/2}}\left(2 - \frac{n_2{}^2}{n_1{}^2}\right)\frac{1}{k_0 r} \qquad \textbf{Equation 2.6}$$

The sensitivity factors for both modes are related to the resonator radius r. For resonators with the same refractive index n_1, their refractive index sensitivities in the same solution are highly dependent on their sizes. In a certain radius range, smaller microspheres have larger sensitivity factors for both TE and TM modes. Therefore, it is easier for them to obtain higher sensitivities. The highest sensitivity achieved was nearly 55 nm/RIU with the microsphere's diameter about 45 μm.

However, it was observed that the sensitivity of microspheres with D∼163 μm was higher than that of microspheres with D∼53 μm. For large microspheres (D > 150 μm), light is more tightly confined inside, further limiting their evanescent tails' extension into the medium. On the other hand, their ultra-large Q-factors can result in much longer effective length at the same time, which helps to increase sensitivity to some extent.

2.6.3 Optimal Size of Silica Microsphere for Sensing Applications

To achieve the best sensing performance of WGM silica microspheres, it is desirable to obtain high Q-factor and high refractive index sensitivity at the same time. These two parameters

are greatly dependent on the diameter of a microsphere. However, the resonator's size affects the Q-factor and the sensitivity in different ways, as discussed in the previous section. Large microspheres have higher Q-factors, making it easier to detect a small resonant wavelength shift; however, their sensitivity is limited. Small microspheres can obtain higher sensitivity, but it is challenging to measure small resonant wavelength change since they have broad resonant peaks. Therefore, it is necessary to find a compromise between these two parameters to optimize the microsphere's sensing performance. Among a variety of silica microspheres analyzed ($D \sim 15 - 165$ μm), resonators with diameter ~ 45 μm obtained the highest Q-factors in air and the highest bulk solution refractive index sensitivity. Although their Q-factors in liquid were not very high, obvious resonant wavelength shifts still could be identified. Therefore, the optimal size of silica microspheres selected in this work is ~ 45 μm for sensing applications.

2.7 Thermal Effects on Microsphere Resonators

2.7.1 Theory of Resonant Wavelength Shifts Caused by Temperature Change

WGM resonators, as label-free optical refractive index sensors, have been applied in various applications. To enhance their performance, it is necessary to reduce as much noise as possible. Among various noise sources that affect a resonator's performance, thermal-induced fluctuation is the main noise.[12] Based on the research discussed in the previous section, it is known that the size and the refractive index of a resonator are important parameters which have great influence on the WGM resonance criterion. However, a resonator's size and refractive index are very susceptible to temperature changes. Large thermal fluctuation may greatly alter the resonator's size and refractive index, leading to appreciable shifts in the resonant wavelength. This can affect the sensing results. Thus, it is necessary to keep a stable and continuous operational environment

when using a resonator[16,17] and checking the temperature influence on the performance of WGM resonators.

Change in microsphere resonator's size and refractive index by temperature fluctuation induces a change in the cavity optical path, which leads to the resonant wavelength shift. The resonator material has a linear thermal expansion coefficient of α (unit:$℃^{-1}$) that is related to the microcavity size and a thermo-optic coefficient β (unit:$℃^{-1}$) which is used to describe the change of its refractive index with temperature. The thermo-optic effect is a result of the competition between the material's absorption resonance change (polarizability) and its density change (thermal expansion) caused by the temperature.[18] For dielectric materials, such as silica, the polarizability is dominant. Therefore, these materials' thermo-optic coefficients have positive values.[19] A wavelength shift in resonance caused by the microsphere's temperature change can be expressed as a function of the resonator's diameter and its refractive index shown in **Eq. 2.7**:[19]

$$\frac{d\lambda}{\lambda} = \frac{d(nD)}{nD} = \frac{dD}{D} + \frac{dn}{n} = \alpha dT + \beta dT = (\alpha + \beta)dT$$

$$\frac{d\lambda}{dT} = \lambda(\alpha + \beta) \qquad \textbf{Equation 2.7}$$

Here λ represents the resonant wavelength; n and D are the refractive index and diameter of a microsphere, respectively; dD, dn and dT are changes of the resonator's diameter, refractive index and temperature, respectively; $\alpha = \frac{\mathrm{dD}}{\mathrm{DdT}}$ is the thermal expansion coefficient, and $\beta = \frac{\mathrm{dn}}{\mathrm{ndT}}$ is the thermo-optic coefficient of the resonator. For fused silica bulk material at 633 nm, $\alpha \approx 0.55 \times 10^{-6}\ ℃^{-1}$, and $\beta \approx 8.9 \times 10^{-6}\ ℃^{-1}$.[20] It is obvious that β is one order magnitude larger than α. Therefore, the temperature has a larger influence on the resonator's refractive index. The resonant wavelength shift is mainly due to the refractive index change of the

resonator.[8] Both coefficients are positive values; hence, when the temperature increases a red shift should be observed for the resonant wavelength. On the other hand, when the surrounding medium is liquid, the refractive index of the liquid will have bigger changes with temperature variation. Because liquids usually have a much larger thermo-optic effect than that of air. The thermo-optic coefficient of water is about $-94 \times 10^{-6}\ ℃^{-1}$ at 633 nm.[20] This negative value will cause a blue shift of the resonant wavelength with increasing temperature, counteracting some of the thermo-optic and thermo-mechanic effects from the resonator itself.[21]

The temperature influence on the resonant wavelength shifts for both barium titanate and fused silica microsphere resonators were investigated in detail as follows.

2.7.2 Experimental Setup for Temperature Study

The experimental setup for this temperature study is shown in **Fig. 2.9**. This setup was very similar to the one utilized in the previous study on resonator size. The 633 nm light was coupled within the resonator through a Dove prism by TIR. An electric heating plate was placed on the Dove prism to heat the sample. The Heat Wave (HW-30, Dagan Corporation), a low electrical noise heating temperature-controller, was used to accurately control the temperature. In order to better reduce environmental disturbance from the room the resonator and water were put in an insulted vial. The thermistor (TH-30, Spare Thermister for HW-30) was placed about 0.4 mm away from the resonator in the vial to monitor the temperature change of the microsphere. The temperature was measured at the same time as the WGM resonant wavelength shifts were recorded.

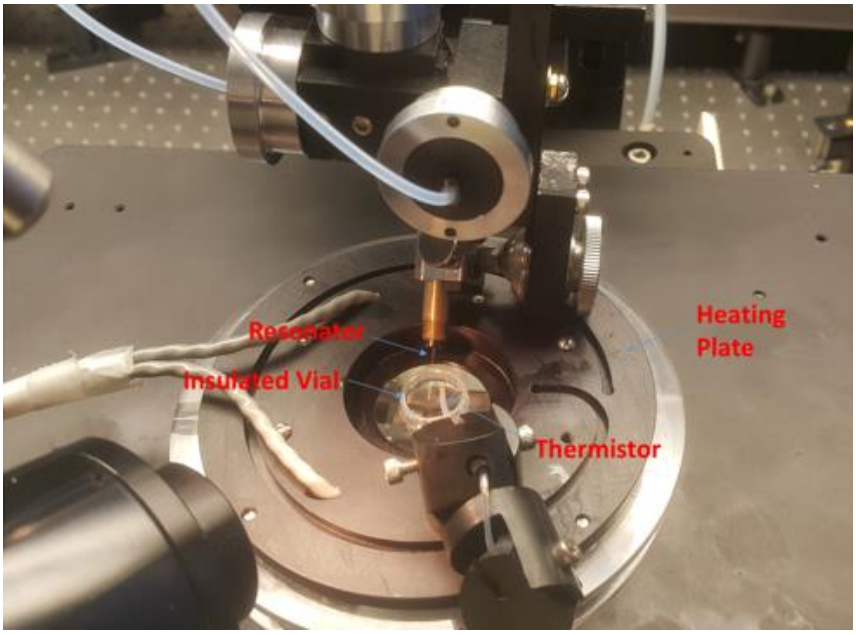

Figure 2.9. The Experimental setup for temperature study of microsphere resonators.

2.7.3 Resonant Wavelength Stability Test at a Constant Temperature

Before studying the temperature effects on the microsphere's resonant wavelength it is necessary to test the stability of the temperature sensor first and also prove the stabilization of resonant wavelength at a constant temperature. In **Fig. 2.10**, the temperature of the thermistor versus time was recorded. The temperature was held constant at 21.4 ± 0.1 ℃ for 1 hour. The extremely stable performance of the thermistor was demonstrated.

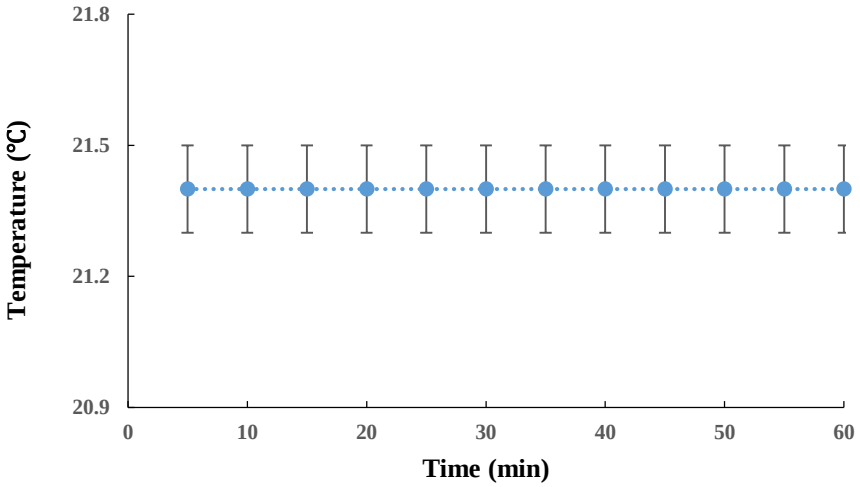

Figure 2.10. Temperature stability test of the thermistor.

Next, the microspheres' resonant wavelength stability at a constant temperature was demonstrated. WGM resonant wavelengths of barium titanate microspheres with diameter of 106 μm and silica microspheres with diameter of 85 μm were monitored at 20.7 ℃ over a 1 hour period. Results are shown in **Fig. 2.11**. Barium titanate glass microspheres were purchased from Mo-Sci Corporation (Rolla, MO). Silica microspheres were fabricated by the same method illustrated in the previous section. The surface tension melted a tapered fiber to form a microsphere with a smooth surface. It was observed that for both kinds of microspheres the maximum resonant wavelength fluctuations were less than 1 pm, which demonstrated the stability of the measurement system. Air convection, room temperature fluctuation and other problems that may affect the stabilization of the experimental setup were not found significant.

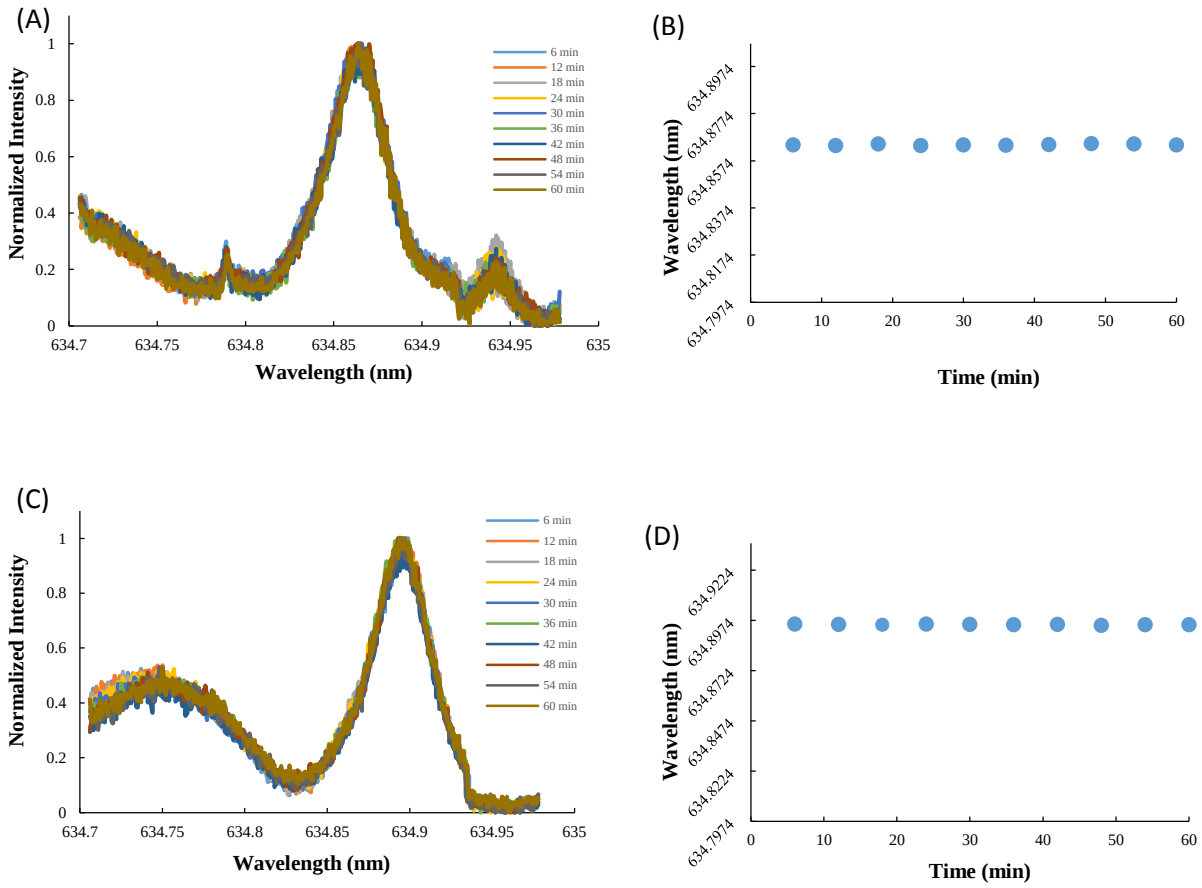

Figure. 2.11. Schematics of microspheres' resonant wavelengths stability in water at 20.7 ℃ for 1 hour. (A) (B) show the resonant wavelength fluctuation of a silica microsphere; its maximum wavelength variation was about 0.8 pm. (C) (D) represent the resonant wavelength fluctuation of a barium titanate microsphere; its maximum wavelength variation was 0.6 pm.

2.7.4 Temperature Effects on Silica Microspheres and Barium Titanate Microspheres with Different Diameters in Water

With the stability of the system demonstrated, the temperature effects on silica microspheres and barium titanate microspheres could be studied in water. The silica microspheres with diameters of 45 μm, 53 μm, 85 μm were fabricated, and barium titanate microspheres with diameters of 45 μm, 75 μm, 106 μm, 125 μm were purchased. A vial was filled with DI water. Then the microsphere and the thermistor were immersed in the water. The measurement started

at room temperature (21 ℃), then the microsphere and the surrounding medium were heated up to about 20 ℃ higher at a rate of 1 ℃ every 3-4 minutes. The temperature was slowly and steadily increased to make sure the resonator and the surrounding medium were in thermal equilibrium. The resonant wavelength against temperature was recorded for every 0.5 or 1 ℃ during the process.

The temperature influence on silica microspheres was studied first. Their temperature sensitivities, linear correlation coefficients, as well as Q-factors in water are listed in **Table 2.3.** To better view the resonant wavelength shifts versus temperature rise, **Fig. 2.12** plots the calibration curves for these different sizes of resonators. The temperature sensitivities (resonant wavelength shift per unit temperature change, nm/℃) were extracted via the curve fitting.

Table 2.3. Temperature influence on silica microspheres with different diameters.
(N=3, all values are average results)

Resonator Diameter (μm)	**Sensitivity** (pm/℃)	**R^2**	**Q-factor**
45 ± 4	2.9 ± 0.1	0.991 ± 0.002	$(5.37 \pm 1.1) \times 10^4$
53 ± 3	3.9 ± 0.1	0.992 ± 0.006	$(1.33 \pm 0.6) \times 10^4$
85 ± 2	5.8 ± 0.2	0.993 ± 0.002	$(3.75 \pm 0.7) \times 10^5$

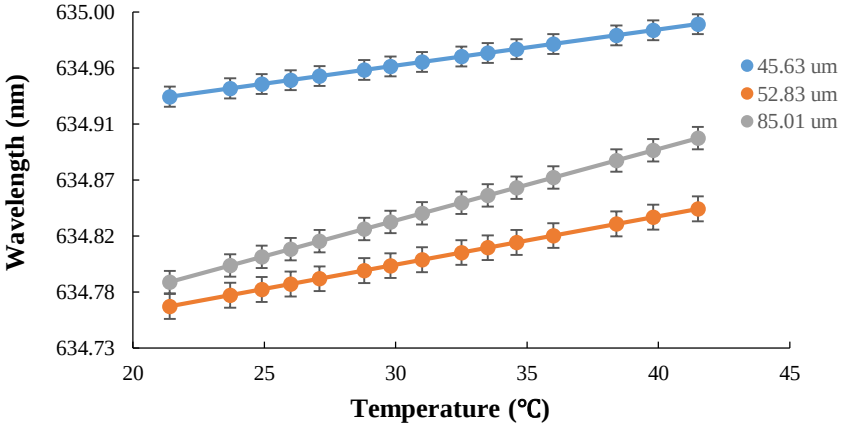

Figure 2.12. Resonant wavelengths versus temperature increase for silica microsphere resonators with different diameters.

Based on **Table 2.3** and **Fig. 2.12**, a linear relationship between the resonant wavelength shifts and the temperature change was observed for all microspheres. At 633 nm, the sum of α and β coefficients of bulk silica materials is about $9.45 \times 10^{-6}\ ℃^{-1}$, leading to a theoretical temperature sensitivity of about 6 pm $℃^{-1}$ (Sensitivity=$\lambda \times (\alpha + \beta)$) in air. However, measured sensitivities of microspheres were smaller than this value, which was due to the thermo-optic effect from water.[22] Water has a negative thermo-optic coefficient β_w of $-94 \times 10^{-6}\ ℃^{-1}$. When the temperature of water increases its refractive index decreases, resulting in a blue shift of the resonant wavelength. This value could be calculated by using **Eq. 2.8**:

$$\boldsymbol{\Delta\lambda = \beta_w \times S} \qquad \textbf{Equation 2.8}$$

Here $\Delta\lambda$ is the blue shift of the resonant wavelength per ℃ caused by the water; β_w is the thermo-optic coefficient of water, and S is the measured solution refractive index sensitivity of the microspheres. As mentioned in the previous section, silica microspheres with different sizes have different S. For microspheres with a diameter in the range of $45 - 105$ μm, smaller resonators have higher S. The S for silica microspheres with diameters of 45 μm, 53 μm, 85 μm are approximately $56\ \mathrm{nm/RIU}$, $30\ \mathrm{nm/RIU}$, $21\ \mathrm{nm/RIU}$, respectively. By using the **Eq. 2.8**, the blue shift $\Delta\lambda$ per ℃ caused by the water's negative thermo-optic effect was calculated. For microspheres with diameters of 45 μm, 53 μm, 85 μm, the corresponding values are 5.26 pm $℃^{-1}$, 2.82 pm $℃^{-1}$ and 1.97 pm $℃^{-1}$, respectively. Therefore, the resonant wavelength shift caused by the contribution of a microsphere's size and refractive index can be estimated. It is the combination of the blue shift by water contribution and the measured combined effect. The measured sum of the microsphere resonators' α + β can be calculated ($\alpha + \beta = \lambda \times$ resonator′s contribution). Results are listed in **Table 2.4**:

Table 2.4. Measured property values of silica microspheres with various sizes (N=3, all values are average results)

Resonator Diameter ($\boldsymbol{\mu m}$)	**Absolute Temperature Sensitivity** ($\boldsymbol{pm}$℃$^{\boldsymbol{-1}}$)	**Measured** $\boldsymbol{\alpha + \beta}$ ($\mathbf{10^{-6}}$ ℃$^{\mathbf{-1}}$)
45 ± 4	8.16 ± 0.5	12.85 ± 0.15
53 ± 3	6.72 ± 1.1	10.59 ± 0.24
85 ± 2	7.72 ± 0.8	12.16 ± 0.18

From **Table 2.4**, a slight variation in the absolute temperature sensitivities was observed between the microspheres with different diameters, since the resonant wavelength was related to the resonator size. Moreover, the measured absolute sensitivities were a little higher than the theoretical value. The main reason could be due to the use of the values α and β.[23] The calculation of the theoretical sensitivity is based on the α and β values of the bulk silica material. However, the calculated sum of α and β coefficients of silica were slightly larger than those of the bulk material. It may be due to the reason that when silica resonators are fabricated in micrometer scale, their α and β coefficients will change slightly. Therefore, for future studies, it will be necessary to further measure the thermal expansion and thermo optic coefficients in micro-scale materials. At the same time as the sensitivities were measured, it was noticeable that the temperature increase did not have much influence on the resonators' Q-factors in water. In addition, larger silica microspheres had higher Q-factors, which was consistent with the previous study. On the other hand, small microspheres have small mode volume, so they are less susceptible to the thermofractive noise.[22] Based on **Table 2.3**, the silica microspheres with a diameter of 45 μm exhibited the minimal temperature sensitivity. This phenomenon indicates that the temperature influence on them is the least, making them good candidates for sensing applications.

The temperature effects on WGM resonant wavelength were also studied for barium titanate ($BaTiO_3$) microsphere resonators. Barium titanate microspheres are crystalline photorefractive WGM resonators with a high refractive index (RI ≈ 1.9). Its bulk material has a thermal expansion coefficient of $10.1 \times 10^{-6}\ ℃^{-1}$.[24] However, its thermo-optic coefficient is still unknown, which may be due to its complex structure. Barium titanate solid can exist in five phases. The same method for silica microspheres was used to analyze the temperature effects on barium titanate microspheres with various diameters. Results are shown in **Table 2.5** and **Fig. 2.13**.

Table 2.5 Temperature influence on barium titante microspheres with different diameters. (N=3, all values are average results)

Diameter of resonator (μm)	Sensitivity ($pm\ ℃^{-1}$)	R^2	Q-factor
45 ± 3	8.4 ± 0.5	0.998 ± 0.001	$(5.60 \pm 0.8) \times 10^4$
75 ± 4	8.0 ± 0.8	0.996 ± 0.002	$(5.16 \pm 0.7) \times 10^4$
106 ± 4	10.9 ± 0.4	0.994 ± 0.004	$(2.09 \pm 0.5) \times 10^4$
125 ± 4	11.3 ± 0.5	0.995 ± 0.002	$(3.41 \pm 0.6) \times 10^4$

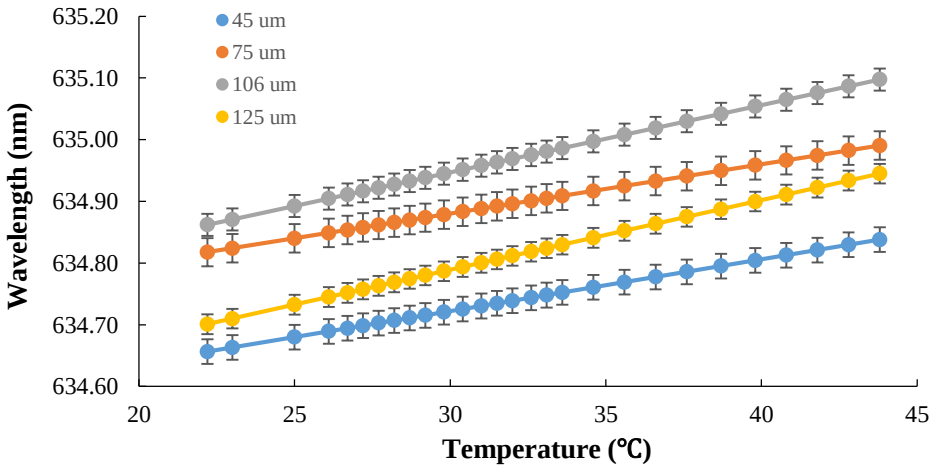

Figure 2.13. Resonant wavelengths versus temperature increase for barium titanate microsphere resonators with different diameters.

From **Table 2.5** it was observed that the measured linear correlation coefficients were all close to 1, indicating an excellent linearity of the resonant wavelength shifts versus temperature rise. This also meant the sum of barium titanate microspheres' thermal expansion coefficient and thermo-optic coefficient were positive and should be regarded as constant values in the measurement range. On the other hand, it was seen that the temperature sensitivities of the barium titanate microspheres were higher than those of the silica microspheres, which could be due to two main factors. First, barium titanate material has a larger sum of the thermal expansion and thermo-optic coefficients. Although its thermo-optic coefficient has not yet been scientifically verified its thermal expansion coefficient itself is already close to the sum of the two coefficients of silica. Second, as WGM resonators, the bulk solution refractive index sensitivity of barium titanate microspheres is about 2-12 nm/RIU, which is lower than that of the silica microspheres. Hence, the resonant wavelength blue shift caused by the water's thermo-optic effect is smaller. In addition, large barium titanate microspheres showed higher temperature sensitivities than those of the small microspheres.

2.7.5 Temperature Effects on Silica Microspheres and Barium Titanate Microspheres with Different Diameters in PBS Solution

Instead of water, a phosphate-buffered saline (PBS) solution of pH~7.4 is used as the medium to research the salt effects on WGM temperature study. PBS is a water-based salt solution with the main component sodium chloride (NaCl). It is a common buffer solution utilized in biological research. The temperature effects in PBS solution were studied for silica microspheres with a diameter of 85 μm and barium titanate microspheres with a diameter of 106 μm. **Figure 2.14** compares the resonators' temperature sensitivities in water and PBS solution. Red shift and linearity were observed for microspheres in PBS solution as well as in water.

However, for both resonators, their temperature sensitivities were a little higher in water. This is probably due to the fact that PBS has a larger negative thermo-optic coefficient than that of water, leading to a bigger blue shift of the resonant wavelength. The exact thermo-optic coefficient of a PBS solution depends on its components. Nevertheless, since NaCl is the main component of a PBS solution, its thermo-optic coefficient should be close to that of a NaCl solution. The thermo-optic coefficient of the 1 mol/L NaCl solution is about $-1.2 \times 10^{-4}\ ^{\circ}\mathrm{C}^{-1}$, compensating for the red shift caused by the resonator properties to a greater degree than that of water.

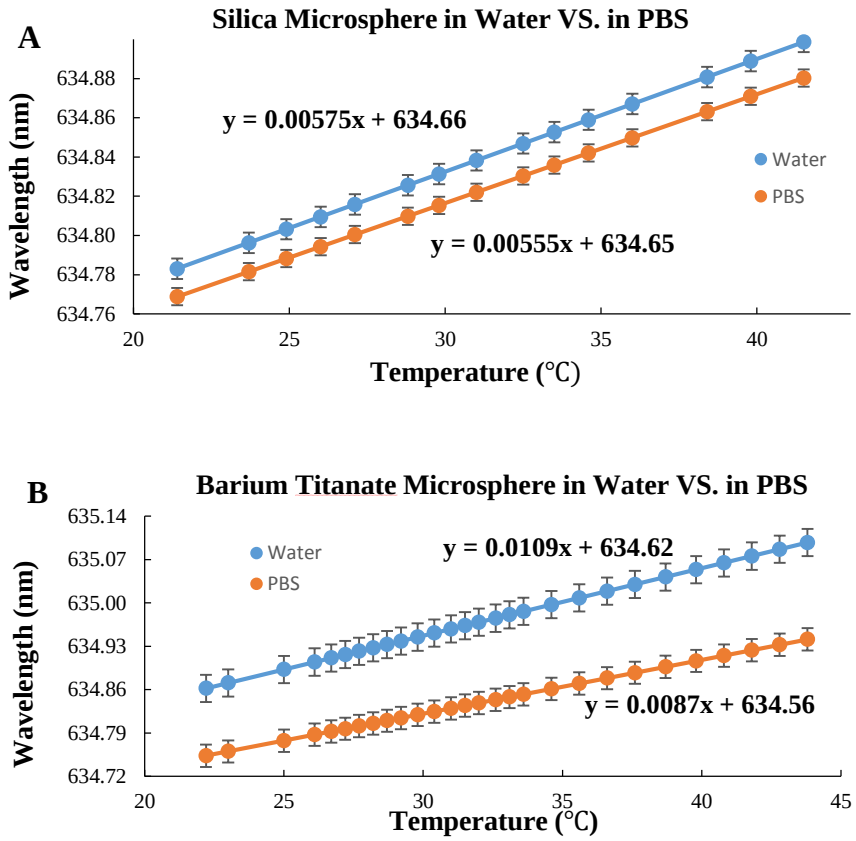

Figure 2.14. (A), (B) illustrate the calibration curves for silica microspheres and barium titanate microspheres in water and in PBS, separately. Smaller temperature sensitivities were observed in the PBS solution for both microspheres, which may be due to the fact that PBS has a larger negative thermo-optic coefficient than that of water, leading to a greater blue shift of the resonant wavelength.

2.7.6 Comparison of the Resonator Heat-Up and Cool-Down Processes

The heat-up and the cool-down processes of silica microspheres and barium titanate microspheres were compared. When the heat up process was finished the heater was turned off and the whole system was allowed to cool down naturally. The results are compared in **Fig 2.15**. In the cool down process linear and blue shifts of the resonant wavelength versus temperature decrease were observed for both resonators. In theory, the behavior for these two processes should be exactly reversible with the same sensitivities. However, the measured temperature sensitivity of the cool down process was a little lower than that of the heat-up process. The difference was about $0.6 - 1.1$ pm $℃^{-1}$. This result may be mainly attributed to the thermal disequilibrium between the resonator and water. The temperature measured by the sensor shows the temperature of the water. However, the temperature decreasing degree of the resonator may be not the same as that of the water. In addition, a small fluctuation exists in the resonant wavelength at a constant temperature, as shown in the previous section 2.7.3. This value was about $0.6 - 0.8$ pm. These two factors may result in the different temperature sensitivities of the heat-up and cool-down processes.

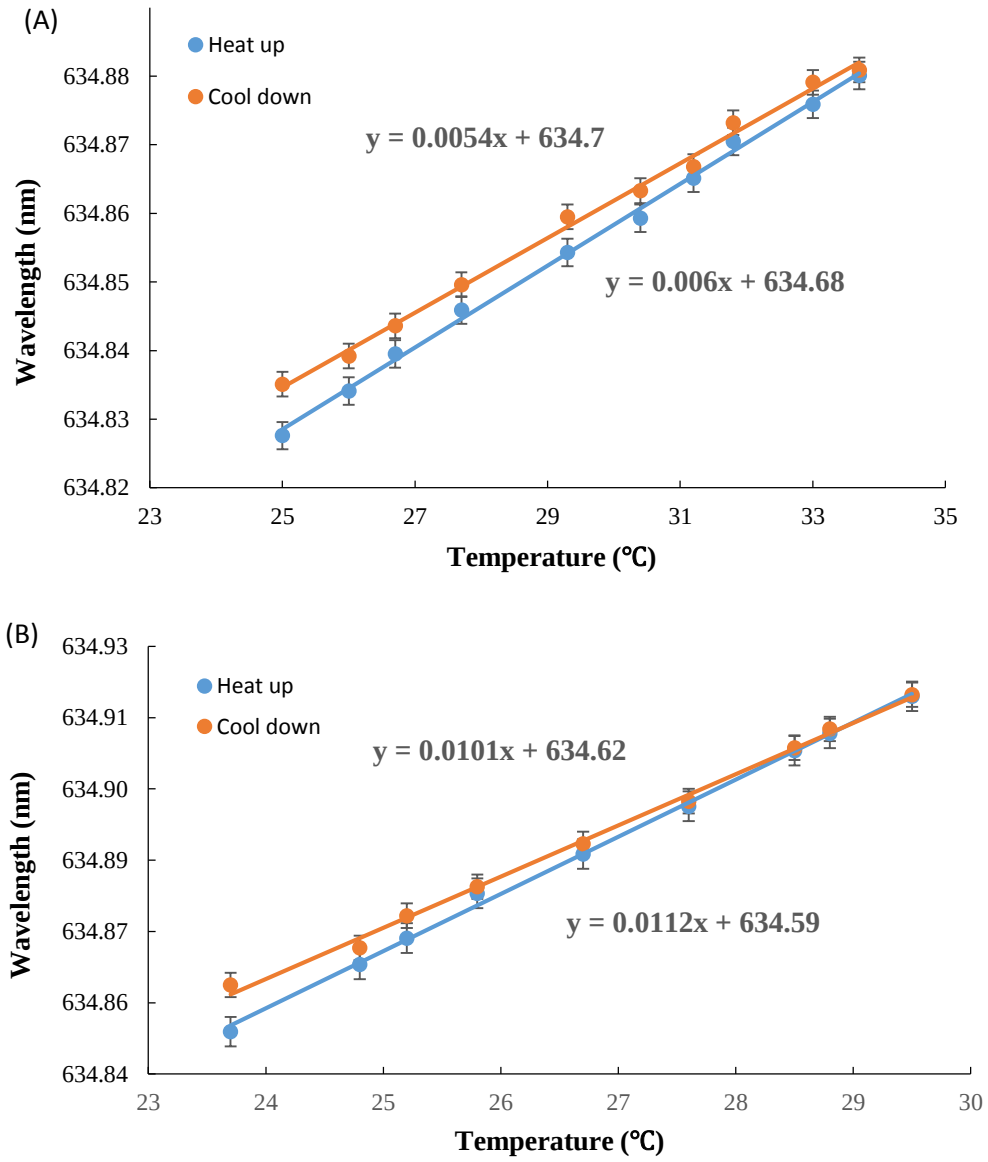

Figure 2.15. Heat-up and cool-down processes for silica microspheres (A) and barium titanate microspheres (B). Slight sensitivity differences were observed between these two processes for each microsphere.

2.8 Incident Light Power Influence on the Silica Microspheres

As discussed in section 2.7 WGM resonant wavelength is easily affected by the thermal fluctuations originating from the ambient environment temperature change. In the meantime, when high incident power is launched into the resonator, light is partially absorbed by its

material. This may also increase the temperature of the microcavity, leading to a resonant wavelength shift. Silica microspheres with different launched light powers were studied. First, a low-power light of about 55 μW was utilized to excite the resonator; a corresponding resonant wavelength was recorded. Then a high-power light of about 260 μW was launched into the microsphere. The resonant wavelength was tracked every 10 minutes. Results are shown in **Fig 2.16**. When the high light power was circulated in the microsphere for 30 minutes only a negligible red shift was observed. This result may be due to the fact that the light absorption by the resonator's material caused the microsphere's temperature increase. In conclusion, the thermal fluctuation due to the high light power launching in a microsphere will not lead to a large change in the resonant wavelength. To decrease noise, it is still necessary to keep the launching light in a constant power when using WGM resonators for sensing applications.

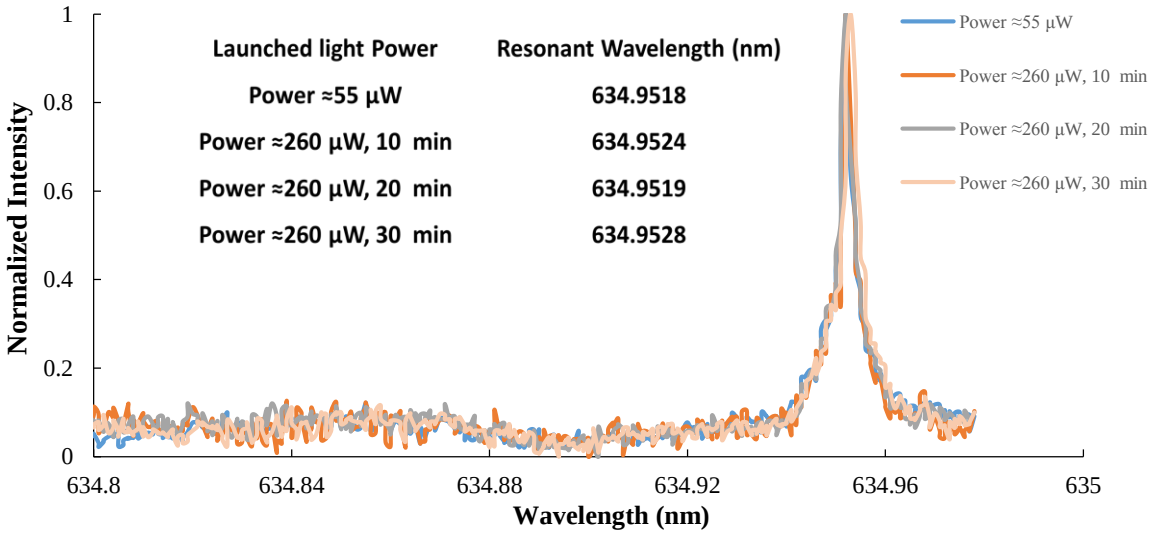

Figure 2.16. Resonant wavelengths of silica microspheres with different launched light power within themselves.

2.9 Conclusions

In this chapter the resonator size effects on silica microspheres and barium titanate were studied. The two important parameters, Q-factor and sensitivity, that describe the performance of a WGM resonator are highly related to its geometry. Silica microspheres with a diameter ~ 45 μm were found to achieve a high Q-factor (1.9×10^6) in air and a high bulk material refractive index sensitivity of around 56 nm/RIU. Meanwhile, thermal influences on silica microspheres and barium titanate microspheres were also studied in different media. Temperature fluctuations can change both the size and the refractive index of microspheres as well as the refractive index of the surrounding medium. Silica microspheres with a diameter of 45 μm exhibited the minimal effect from temperature changes, making them good candidates for biosensing applications. In addition, barium titanate microspheres showed high temperature sensitivity in liquid (~ 10 pm/°C). Therefore, they may be used as sensitive temperature sensors in future work.

2. 10 References

1. Righini, G. C.; Soria, S., Biosensing by WGM Microspherical Resonators. *Sensors (Basel)* **2016,** *16* (6).
2. Hanumegowda, N. M.; White, I. M.; Fan, X. In *Aqueous mercuric ion detection with microsphere optical resonator sensors*, American Institute of Chemical Engineers: 2005; pp 563b/1-563b/8.
3. Vollmer, F.; Arnold, S., Whispering-gallery-mode biosensing: label-free detection down to single molecules. *Nat. Methods* **2008,** *5* (7), 591-596.
4. Hunt, H. K.; Armani, A. M., Label-free biological and chemical sensors. *Nanoscale* **2010,** *2* (9), 1544-1559.
5. Arnold, S.; Khoshsima, M.; Teraoka, I.; Holler, S.; Vollmer, F., Shift of whispering-gallery modes in microspheres by protein adsorption. *Opt. Lett.* **2003,** *28* (4), 272-274.
6. Hanumegowda, N. M.; White, I. M.; Oveys, H.; Fan, X., Label-free protease sensors based on optical microsphere resonators. *Sens. Lett.* **2005,** *3* (4), 315-319.
7. Kippenberg, T. J. A. Nonlinear optics in ultra-high-Q whispering-gallery optical microcavities. 2004.
8. Guan, G.; Arnold, S.; Otugen, M. V., Temperature Measurements Using a Microoptical Sensor Based on Whispering Gallery Modes, *ALAA JOURNAL*. **2006,** 44 (10), 2385-2389.
9. Teraoka, I.; Arnold, S.; Vollmer, F., Perturbation approach to resonance shifts of whispering-gallery modes in a dielectric microsphere as a probe of a surrounding medium. *J. Opt. Soc. Am. B* **2003,** *20* (9), 1937-1946.
10. Gamba, J. The Role of Transport Phenomena in Whispering Gallery Mode Optical Biosensor Performance. **2012**.

11. Foreman, M. R.; Jin, W.-L.; Vollmer, F., Optimizing detection limits in whispering gallery mode biosensing. *Opt Express* **2014,** *22* (5), 5491-511.
12. White, I. M.; Fan, X., On the performance quantification of resonant refractive index sensors. *Opt Express* **2008,** *16* (2), 1020-8.
13. Mortensen, N. A.; Xiao, S.; Pedersen, J., Liquid-infiltrated photonic crystals: enhanced light-matter interactions for lab-on-a-chip applications. *Microfluid. Nanofluid.* **2008,** *4* (1-2), 117-127.
14. Rindorf, L.; Bang, O., Highly sensitive refractometer with a photonic-crystal-fiber long-period grating. *Opt. Lett.* **2008,** *33* (6), 563-565.
15. Reynolds, T.; Henderson, M. R.; Francois, A.; Riesen, N.; Hall, J. M. M.; Afshar, S. V.; Nicholls, S. J.; Monro, T. M., Optimization of whispering gallery resonator design for biosensing applications. *Opt Express* **2015,** *23* (13), 17067-76.
16. Liang, W.; Huang, Y.; Xu, Y.; Lee, R. K.; Yariv, A., Highly sensitive fiber Bragg grating refractive index sensors. *Appl. Phys. Lett.* **2005,** *86* (15), 151122/1-151122/3.
17. Suter, J. D.; White, I. M.; Zhu, H.; Fan, X., Thermal characterization of liquid core optical ring resonator sensors. *Appl Opt* **2007,** *46* (3), 389-96.
18. Righini, G. C.; Dumeige, Y.; Feron, P.; Ferrari, M.; Conti, G. N.; Ristic, D.; Soria, S., Whispering gallery mode microresonators: fundamentals and applications. *Riv. Nuovo Cimento Soc. Ital. Fis.* **2011,** *34* (7), 435-488.
19. Pokrass, M.; Burshtein, Z.; Gvishi, R., Thermo-optic coefficient in some hybrid organic/inorganic fast sol-gel glasses. *Opt. Mater. (Amsterdam, Neth.)* **2010,** *32* (9), 975-981.

20. Rose, B. A.; Maker, A. J.; Armani, A. M., Characterization of thermo-optic coefficient and material loss of high refractive index silica sol-gel films in the visible and near-IR. *Opt. Mater. Express* **2012,** *2* (5), 671-681.
21. Fan, X.; White, I. M.; Shopova, S. I.; Zhu, H.; Suter, J. D.; Sun, Y., Sensitive optical biosensors for unlabeled targets: A review. *Anal. Chim. Acta* **2008,** *620* (1-2), 8-26.
22. Ma, Q.; Rossmann, T.; Guo, Z., Temperature sensitivity of silica micro-resonators. *J. Phys. D: Appl. Phys.* **2008,** *41* (24), 245111/1-245111/6.
23. Foreman, M. R.; Jin, W.-L.; Vollmer, F., Optimizing detection limits in whispering gallery mode biosensing. *Opt Express* **2014,** *22* (5), 5491-511.
24. Schubert, J.; Trithaveesak, O.; Petraru, A.; Jia, C. L.; Uecker, R.; Reiche, P.; Schlom, D. G., Structural and optical properties of epitaxial BaTiO3 thin films grown on GdScO3(110). *Appl. Phys. Lett.* **2003,** *82* (20), 3460-3462.

Chapter 3

Application of Whispering Gallery Mode Silica Microsphere Resonators in the Detection of Biomolecules

3.1 Introduction:

Label-free optical sensors are a convenient and powerful tool which has a number of applications in many areas, such as pharmaceuticals, biomolecule detection, and environmental analysis.[1] The label-free sensing platform enables detection of target molecules in their original forms. It avoids labeling or altering the target molecules, which is easier and cheaper to perform compared with label sensors.[2] For optical biosensors, a common detection mechanism is the measurement of the refractive index change caused by a molecule binding event. For sensing, biorecognition molecules are immobilized onto the surface of an optical biosensor first, then the sensor is immersed in a buffer solution. When target molecules which have a larger refractive index than that of the buffer solution molecules (for example, the refractive index of protein is approximately 1.5 and that of PBS buffer solution is about 1.33) bind to the biorecognition molecules on the sensor's surface, the refractive index near the sensor surface is increased. **Figure 3.1** shows an example of the binding process.

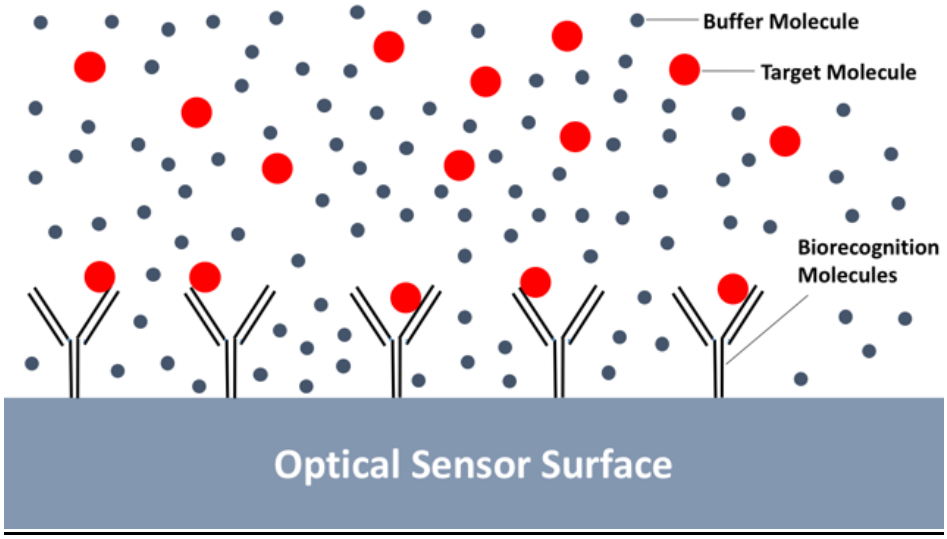

Figure. 3.1. Illustration of an optical label-free biosensor. Target molecules (red) bind to biorecognition molecules (black).

Among various optical biosensors, whispering gallery mode (WGM) microsphere resonators have been widely studied and developed during the past 15 years due to their easy fabrication, simple structure, low-cost, and high sensitivity.[3-8] Light is coupled inside a microsphere via total internal reflection, which creates an evanescent field with a characteristic length of several hundreds of nanometers to strongly interact with the surrounding medium. Therefore, when the surface of the microsphere resonator is functionalized with some molecules that can bind specific analytes, the capture of the target biomolecules will cause a local change in refractive index. It alters the resonant wavelength, allowing highly sensitive and label-free detection of biomolecules.[8]

In this work, the Langmuir-Blodgett approach was used to transfer DOPC-GM1 bilayers on silica microsphere resonator surfaces. Those microspheres were fabricated by the surface tension method as discussed in chapter 2. Since cholera toxin (CT) molecules specifically bind to GM1, the refractive index of the bilayer changes as CT is adsorbed on the resonator's surface, which

causes a WGM resonant wavelength shift. By tracking the total WGM wavelength shift, the maximum characteristic concentration of CT that binds to GM1 can be determined.

3.2 Mechanism for Cholera Toxin Binding to GM1

The binding event of CT to GM1 is a multivalent ligand-receptor interaction. GM1 is a typical ganglioside (glycosphingolipids that contains sialic acid) of mammalian brains, which is located in the epithelial cell apical membrane.[9] The chemical structure of GM1 is shown in **Fig. 3.2**. GM1 has a hydrophilic pentasaccharide chain and a hydrophobic lipid moiety.

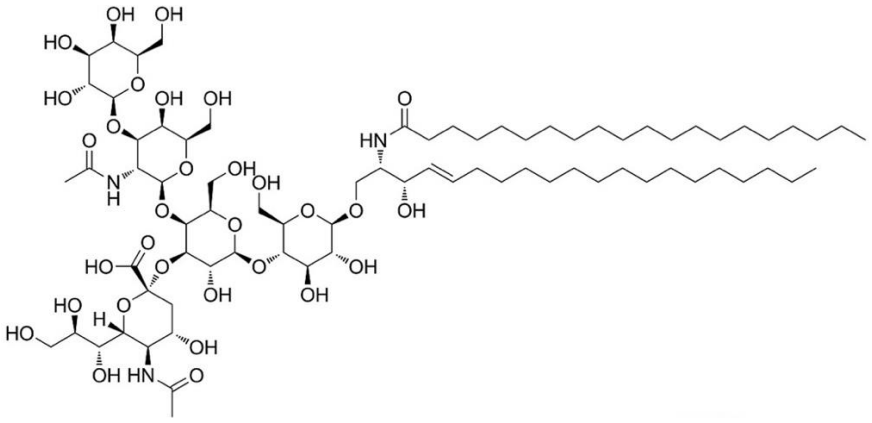

Figure 3.2. Structure of the GM1 ganglioside.

CT is a multimeric protein toxin secreted by the bacteria Vibrio cholera. CT is the main pathogenesis for cholera.[10,11] Cholera is a common disease that affects human being's life. Every year there are approximately 1.3 to 4 million cases of cholera occur around the whole world, and about 21,000 to 143,000 deaths due to cholera.[12] Therefore, it is of great importance to reduce the CT toxicity. CT has an AB_5-type structure: one A subunit (CT-A) that produces the A1-chain with catalytic property to activate adenylyl cyclase[13] and five identical B subunits (CT-B) which can specifically bind to GM1, as illustrated in **Fig. 3.3**.[14,15] The binding constant is about

10^{-8}-10^{-12} M.[16,17] The binding of CT to GM1 is the fist step to cause cholera.[13] Therefore, it is of great interest to study this event.

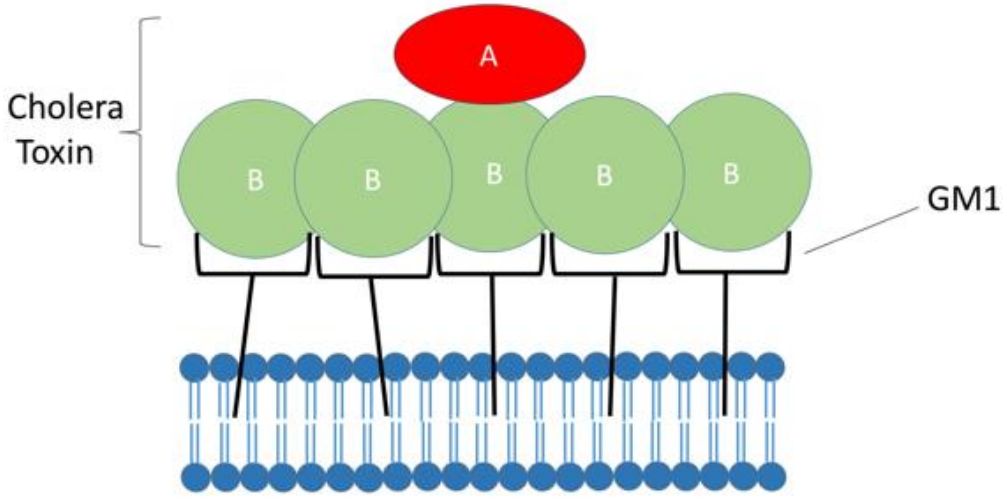

Figure 3.3. The B subunits of Cholera Toxin bind to GM1.

3.3 Langmuir-Blodgett Film Technique

A Langmuir-Blodgett trough (Type 611, Nima Technology, Coventry, England) was utilized to form and transfer DOPC/GM1 bilayers onto the surface of a silica microsphere. Before discussing how the WGM resonator was used to study the binding event of CT to GM1, it is first necessary to understand the Langmuir-Blodgett film technique.

Langmuir-Blodgett films are composed of surfactants that remain trapped between two phases, such as air-water interface. Surfactants are amphiphilic molecules which consist of hydrophobic tails and hydrophilic heads. Hydrophobic groups are nonpolar, such as hydrocarbon chains. Hydrophilic groups are polar, such as hydroxyl groups (-OH), carbonyl groups (-COOH), amino groups ($-NH_2$), and sulfhydryl groups (-SH). The hydrophobic tails of surfactants are oriented towards the air and the hydrophilic heads are more favorable to the polar phase. When

the surfactant molecules are trapped at the air-water interface, their arrangement is shown in **Fig 3.4**.

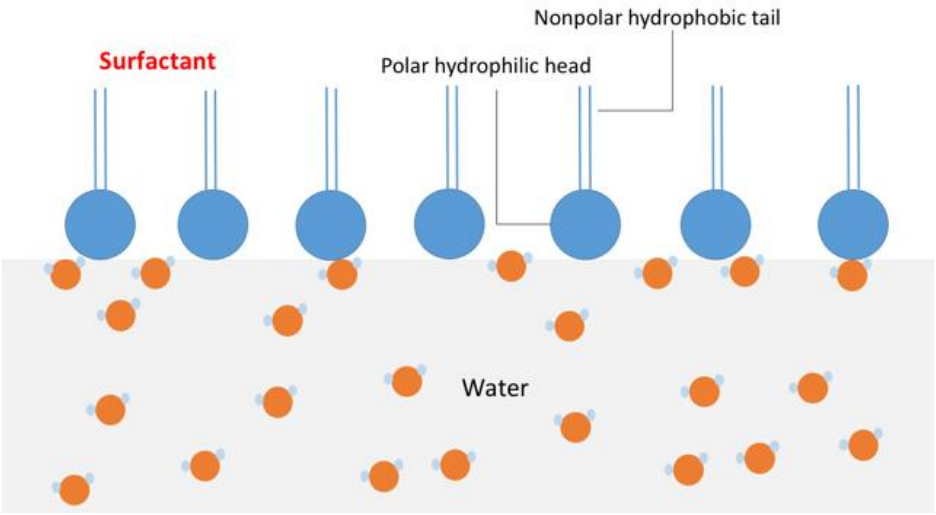

Figure 3.4. Surfactant molecules arrange at an air–water interface.

Surfactants are dissolved in a non-aqueous volatile solvent (e.g. chloroform, methanol). There should be no interaction between the surfactants and the solvent. The solvent is injected onto the polar liquid surface and allowed to evaporate until all the surfactants are totally spread at the liquid-air interface with their tails oriented to the air and heads solvated in the liquid. At first, surfactants spread in a disordered way at the liquid-air interface. When compressing the interface with a barrier, the surface pressure, which is the reduction of the surface tension, increases, making the surfactants pack more closely and in a more ordered way. During the whole compression process the molecular configuration may undergo 5 transitions: Gas (G), Liquid Expanded (LE), LE-LC coexistence phase, Liquid Condensed (LC) and Solid (S), such as DPPC monolayer. An example of a common pressure-area isotherm is shown in **Fig. 3.5 (A)**. However, for the lipid DOPC used in this study, the LE-LC coexistence phase does not exist in

the isotherm, illustrated in **Fig. 3.5 (B)**. With continued compression of the interface, the surface pressure reaches the collapse pressure, which is the maximum surface pressure that a monolayer can be compressed before buckling. Therefore, an appropriate target pressure needs to be chosen to make Langmuir-Blodgett films.

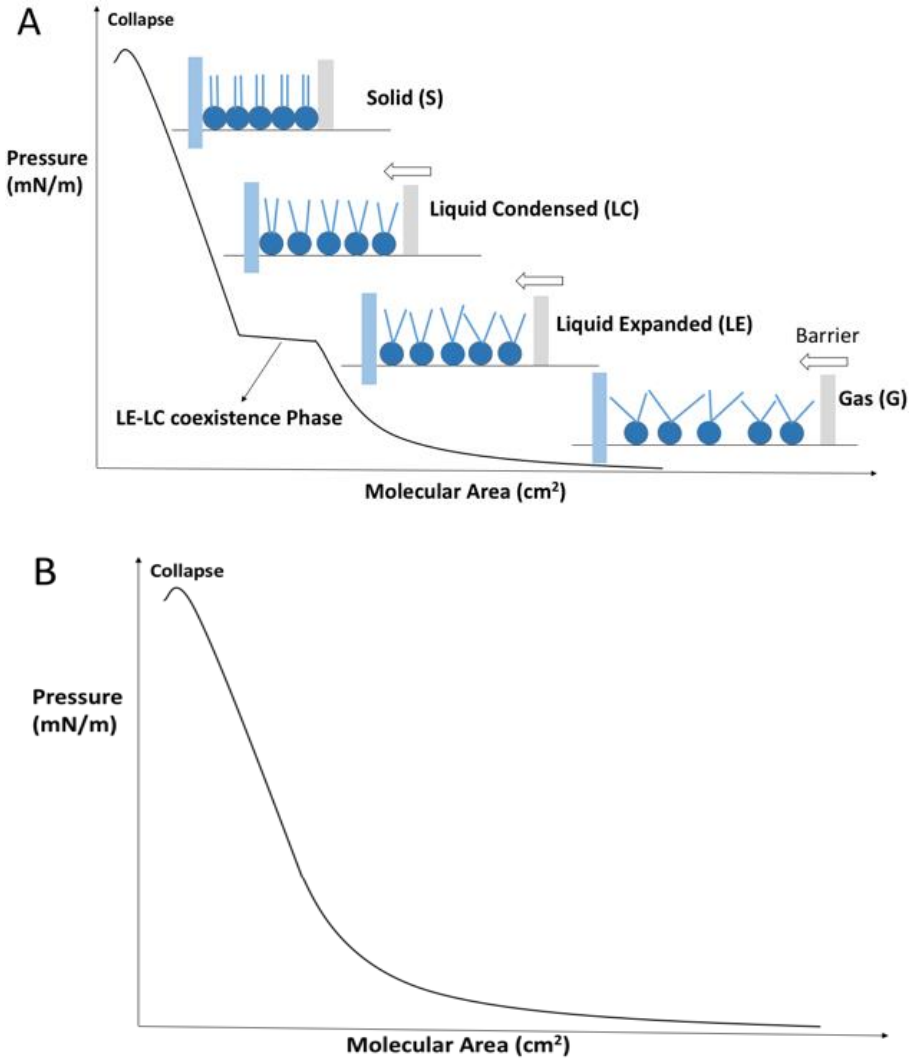

Figure 3.5. (A) An example of the surface-pressure isotherm with 5 regions: Gas (G), Liquid Expanded (LE), LE-LC coexistence phase, Liquid Condensed (LC) and Solid (S). **(B)** A DOPC pressure-area isotherm without the LE-LC coexistence phase. (Both isotherms are cartoon, instead of real pressure-area isotherms)

In order to form a Langmuir-Blodgett film, surfactants are distributed on the interface first, then isotherm cycles are performed. After that, the film is compressed to reach the target pressure and the pressure is held for 10-15 min. By slowly pulling a substrate immersed in the liquid through the monolayer, a film is transferred onto the substrate. In order to form a bilayer, the substrate is dipped back through the film at the air/water interface. **Figure 3.6** illustrates the process of a Langmuir-Blodgett monolayer and bilayer formation.

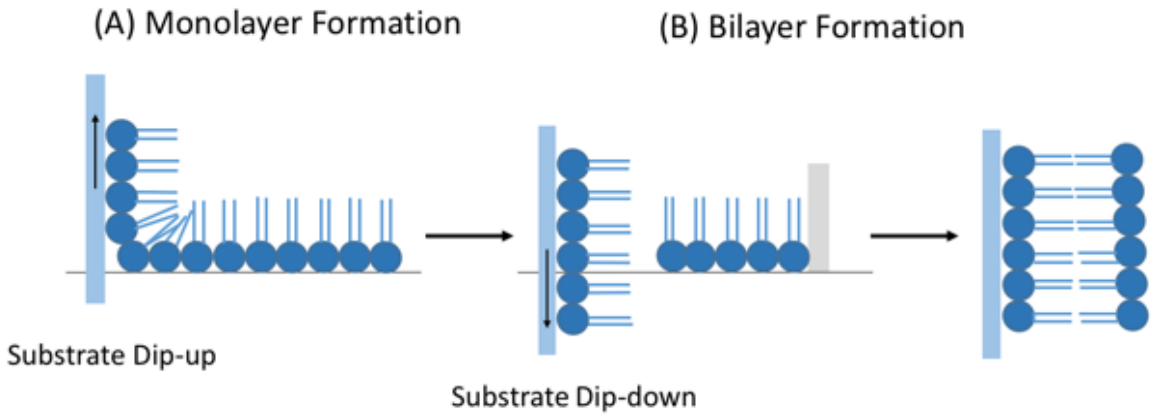

Figure 3.6. Deposition of a monolayer (A) and a bilayer (B) onto a substrate.

3.4 Transfer of DOPC/GM1 Bilayers onto WGM Silica Microsphere Resonators

In this study DOPC/GM1 bilayers were transferred onto WGM resonators to study the binding event of CT to GM1. Silica microspheres with a diameter of 45 μm were utilized as WGM resonators. They were fabricated by the method described in the previous section via surface tension. The stem of a silica microsphere was stably held by the dipper and slowly moved down until the sphere was totally immersed in the subphase of the trough. The microsphere was used as the substrate for deposition of Langmuir-Blodgett films.

DOPC and GM1 were purchased from Avanti Polar Lipids, Alabaster, AL. CT was purchased from Molecular Probes, Eugene, OR. All chemicals were used without further purification. The CT solution was diluted in a PBS solution (pH=7.4) with required concentrations. DOPC/GM1(95:5 mol%) solutions were prepared at 2 mg/ml concentrations in a 65:35 volume mixture of chloroform and methanol. Approximately 30 µl of the lipid solution was injected into the Langmuir-Blodgett trough with an 18 MΩ water subphase. The solvent was allowed to evaporate for 15 minutes before the compression/expansion cycles. Two cycles were performed between the surface pressures of 3 mN/m and 40 mN/m at a constant barrier rate of 100 cm^2/min. Then the film was compressed to 25 mN/m and held for 10 minutes.

By pulling the microsphere at a velocity of 3 mm/min through the monolayer, a DOPC/GM1 monolayer was transferred onto the resonator surface. In order to form a bilayer, the microsphere was dipped back through the film at the air/water interface again. A microsphere coated with DOPC/GM1 bilayer is illustrated in **Fig. 3.7.** In this study, CT only binds to GM1 in the second layer.

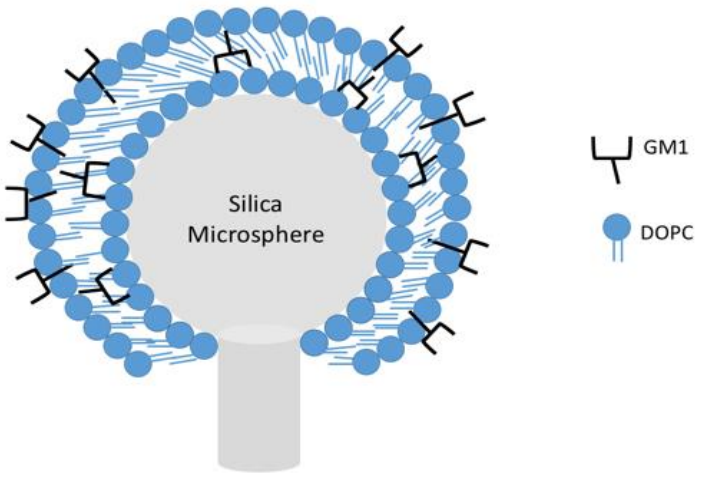

Figure 3.7. A DOPC/GM1 bilayer is coated on the surface of a silica microsphere. The GM1 molecules are embedded in the DOPC second layer.

3.5 Results and Discussion

3.5.1 Demonstration of a DOPC/GM1 Bilayer Transfer onto a Silica Microsphere

Before carrying out the WGM response study of the GM1-cholera toxin binding event, it was necessary to prove that the DOPC/GM1 bilayers were successfully transferred onto the surface of microspheres. The first monolayer was deposited on the microspheres by using the method described above. Then 0.25 mol% Texas-Red dihexadecanoyl-sn-glycero-3-phosphoethanolamine (TR-DHPE) (Life Technologies, Carlsbad, CA) was added to the DOPC/GM1 lipid mixture as a fluorescent lipid probe. This new lipid solution was dispersed onto the water subphase, and the same procedures were performed to transfer the second layer onto the microsphere's surface, forming a bilayer. **Figure. 3.8** illustrates the fluorescence image of a silica microsphere with bilayer transferred using the described procedure. Bright fluorescence was observed on the microsphere, which demonstrated that the DOPC/GM1 bilayer was successfully transferred onto the microsphere's surface.

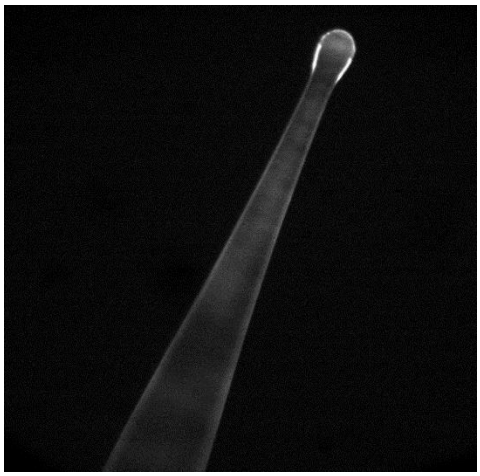

Figure 3.8. Fluorescent image of a silica microsphere coated with DOPC/GM1 bilayer.

3.5.2 Confirmation of Cholera Toxin Binds to GM1 on Silica Microspheres

In order to confirm that CT specially binds to the GM1 in the DOPC/GM1 bilayer, a control experiment was conducted using silica microspheres coated with pure DOPC bilayers. Those resonators were allowed to react with different concentrations of CT solutions for 5 minutes. Since the CT molecules are fluorescently labeled with dye Alexa 555, if they bind onto the microsphere's surface, an increase in fluorescence should be observed when increasing the CT solution concentration (0 pM, 30 pM, 100 pM CT solutions). However, no obvious changes were seen, indicating that nearly no CT molecules bound onto the surface of microspheres coated with pure DOPC bilayers.

On the contrary, when silica microspheres coated with DOPC/GM1 (GM was 5 mol%) bilayers were also allowed to interact with the CT solutions for 5 minutes, noticeable fluorescence was observed, as shown in **Fig. 3.9**. This demonstrates that the increase in fluorescence observed is caused by the specific interaction between the CT and GM1.

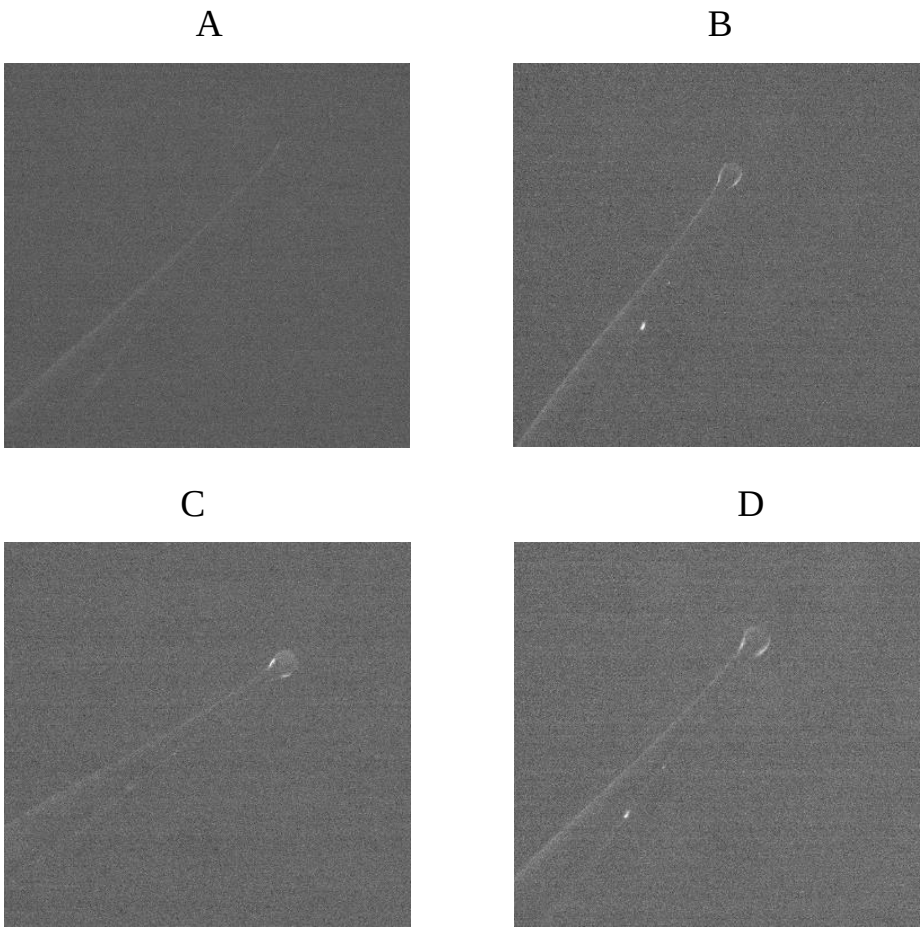

Figure 3.9. Fluorescent images of the same silica microsphere coated with DOPC/GM1(GM1 is 5 mol%) bilayers incubation with (A) 0 pM CT; (B) 10 pM CT; (C) 30 pM CT; (D) 100 pM CT. The increase in fluorescence indicates the specific binding of CT molecules at GM1 sites in DOPC/GM1 bilayers.

By analyzing the light intensity of the microsphere surface versus the CT solution concentration in **Fig. 3.10**, it was obvious that the exposure of the DOPC/GM1 bilayer coated microsphere to CT solutions with the increased concentration led to an increase in the fluorescent intensity. This further indicated that more CT molecules bound to GM1. Meanwhile, it was also observed that the fluorescence intensity leveled off when the concentration of CT solution increased from 30 pM to 100 pM. This may be due to the saturation of CT-GM1 binding sites.

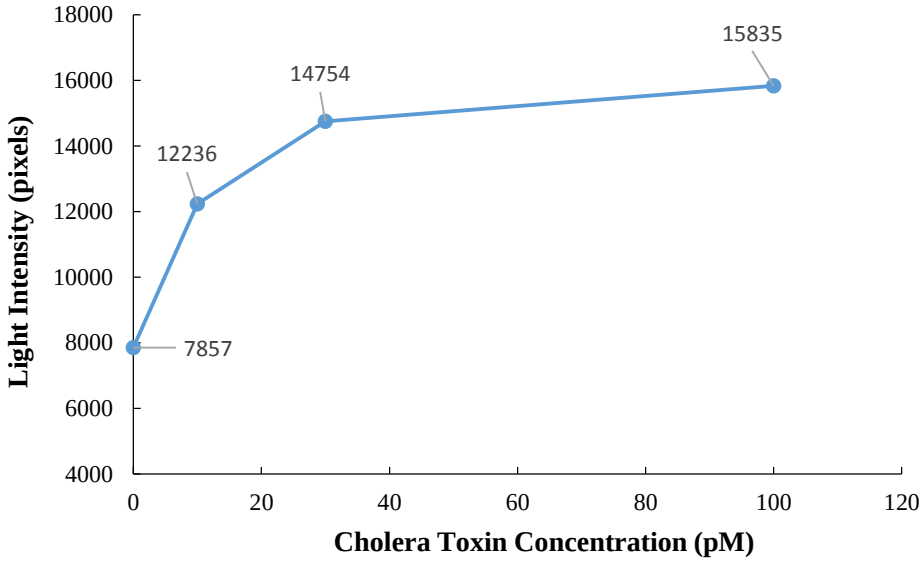

Figure 3.10. Light intensity of the microsphere surface at different CT concentrations. Increased light intensity was observed for higher CT concentration, due to the fact that more CT molecules bound to GM1. When the binding event was nearly saturated, there was no big change in light intensity with the increasing CT concentration.

3.5.3 WGM Response of the DOPC/GM1 Bilayer Coated Silica Microsphere Resonator

Having verified that CT specifically binds to the GM1 in the DOPC/GM1 bilayers, WGM response was explored to detect the presence of CT via the silica microsphere resonators coated with DOPC/GM1 bilayers. For this study, DOPC/GM1 bilayers with 5 mol% GM1 were transferred onto silica microspheres in a diameter about 45 μm. A series of WGM resonant wavelengths were collected as a function of CT concentration, as shown in **Fig 3.12**. Before adding CT solution, this microsphere resonator had a resonant wavelength of 634.8829 nm with a Q-factor of 2.6×10^4. This Q-factor was very close to the Q-factor of silica microspheres with a diameter of 45 μm in liquid solutions ($\sim 10^4$). This indicates that the transfer of DOPC/GM1 bilayer onto the silica microsphere does not have obvious influence on the resonator's Q-factor. When adding 6.1 pM CT, the resonant wavelength had a red shift of 6 pm

as CT binds to the GM1/DOPC bilayer on the microsphere surface. This binding event increases the effective refractive index around the microsphere, leading to the resonant wavelength change. With continued increasing the CT concentration, the resonant wavelength keeps red shifting.

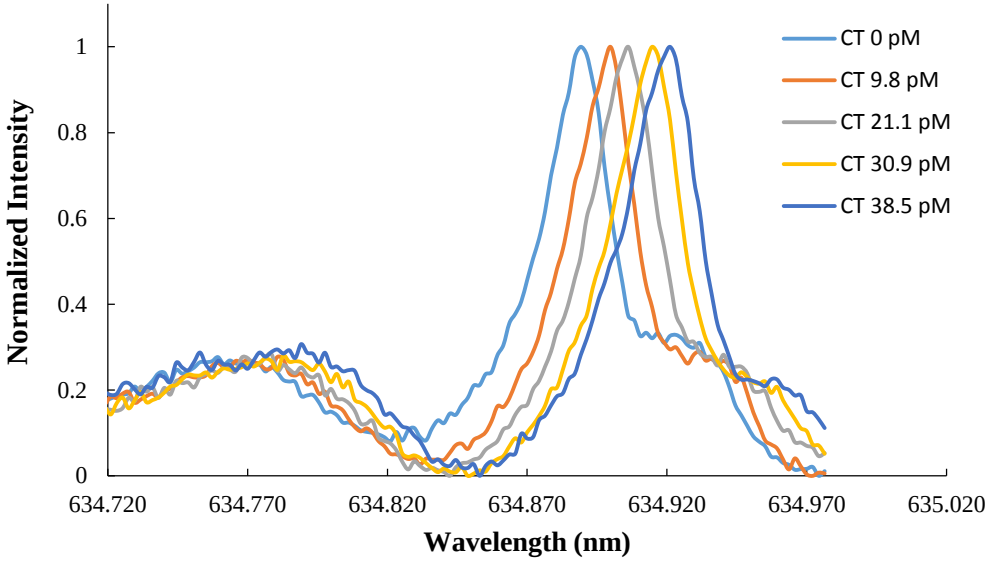

Figure 3.11. WGM resonant wavelengths of the same silica microsphere resonator at CT solution with 5 different concentrations. The specific binding of CT to the GM1 in the DOPC/GM1 bilayer coated on the microsphere changes the effective refractive index around the microsphere, leading to the red shift of the resonant wavelength.

A binding curve which summarizes the results in **Fig. 3.11** is shown in **Fig. 3.12**. This curve describes the WGM resonant wavelength shifts as a function of CT concentration. At the beginning, a linear relationship is exhibited between the WGM shift and the CT concentration (Figure 3.13 (A)). With continued increasing the CT concentration, no obvious shifts are observed, due to the binding saturation. The saturation concentration is approximately 50 pM CT (Figure 3.13 (B)) and a measured K_d is 1.58×10^{-11}(Figure 3.13 (C)). This value is in the range

of the reported K_d values ($7.3 \times 10^{-10} - 4.6 \times 10^{-12}$) obtained by surface plasmon resonance,[12,13] which further confirms the binding event between GM1 and CT.

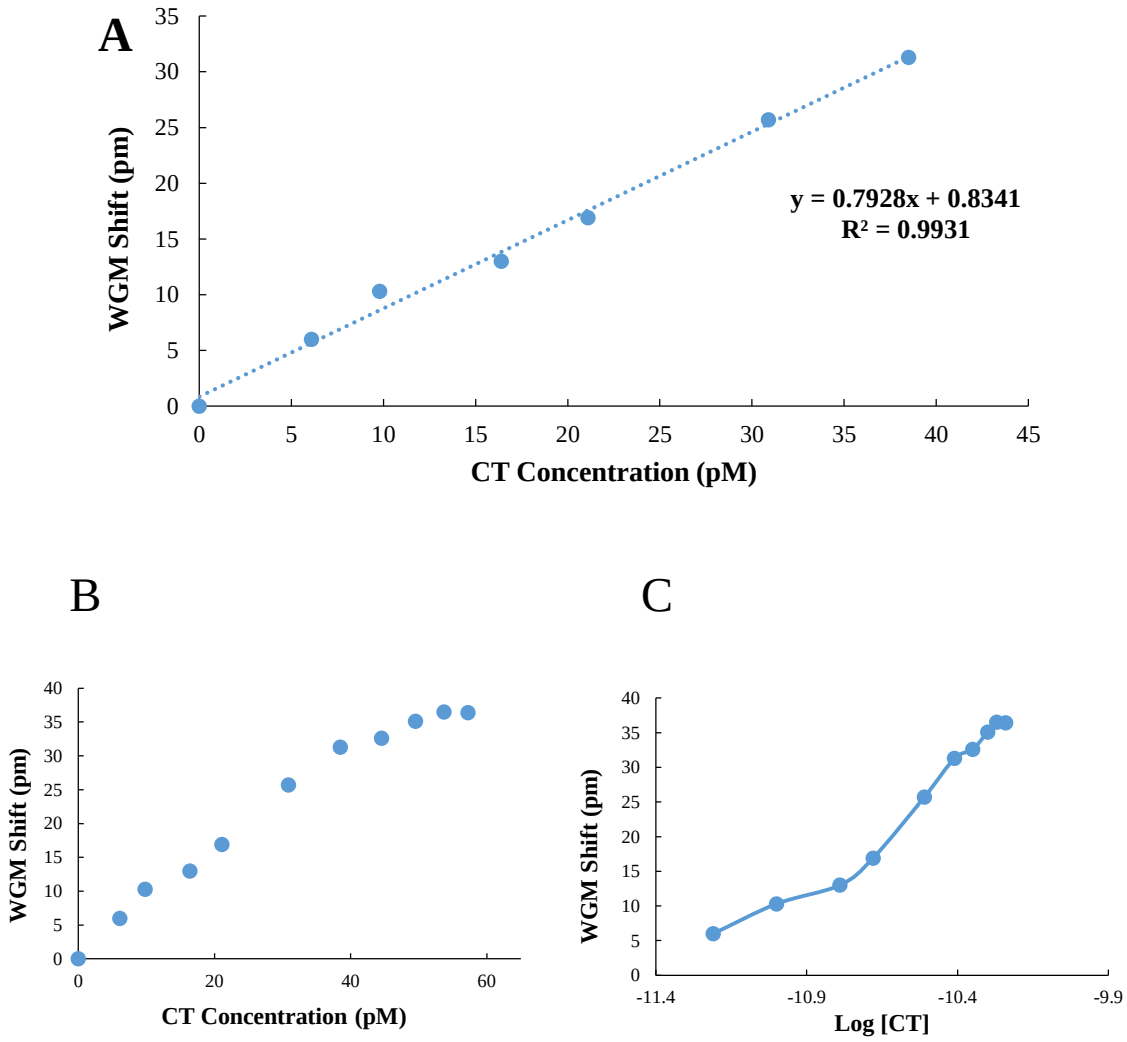

Figure 3.12. CT-GM1 binding event was monitored by tracking the WGM resonant wavelength shifts with increasing the CT concentration. **(A)** A linear relationship (R^2=0.9931) is shown between the CT concentration (0-38.5 pM) and the WGM shift. (B) With continued increasing the CT concentration, no obvious WGM shift is observed ([CT] > 53.7 pM), due to the binding saturation. (C) A log plot of the CT concentration versus WGM shifts, a K_d of 1.58×10^{-11} is calculated from this figure, which is in the range of the reported K_d values ($7.3 \times 10^{-10} - 4.6 \times 10^{-12}$).

The number of CT molecules binds to GM1 is related to the amount of GM1 in GM1/DOPC bilayer coated on the surface of a silica microsphere resonator. Therefore, the next section studied the effects of the density of GM1 in the bilayer on CT-GM1 binding event.

3.5.4 Relationship Between GM1 Concentration and WGM Response

Several different concentrations (5, 6, 7.6, 10, 15.24 mol%) of GM1 in GM1/DOPC bilayers were explored to study the WGM response. All the experimental conditions were kept the same, only the GM1 concentration was varied. The results are shown in **Table 3.1**.

Table 3.1 GM1 concentration effects on WGM response.
(N=3, all values are average results)

GM1 Concentration (mol%)	Sensitivity (pm/pM)	Saturated Concentration (pM)	Total WGM Shift (pm)
5	0.793 ± 0.039	50 ± 1.4	35.7 ± 2.1
6	0.802 ± 0.041	54 ± 2.1	37.5 ± 2.2
7.6	0.782 ± 0.037	59 ± 3.1	48.5 ± 1.3
10	0.593 ± 0.031	16 ± 1.2	9.6 ± 1.1
15.24	0.539 ± 0.025	10 ± 0.8	6.3 ± 0.5

For GM1 concentration in the range of 5-7.6 mol%, the microsphere resonators have similar sensitivities due to their similar sizes. More GM1 in DOPC/GM1 bilayers can bind more CT molecules, leading to a higher CT saturated concentration and a larger total WGM shift. However, with continued increasing the GM1 concentration (GM 1 concentration is 10 mol% and 15.24 mol%), lower sensitivities are observed and less CT binds to GM1 with smaller total WGM shift. This phenomenon may be mainly caused by the GM1 clustering, which inhibits CT binding onto the lipid bilayer. As illustrated in the previous section, CT-GM1 binding is a

multivalent ligand-receptor interaction. For each CT molecule, its five B sites can bind to 5 GM1 molecules. In multivalent interaction ligand density has a significant effect on the binding efficiency.[18,19,20,21,22] The amount of ligands determines their distribution and the distance between each ligand.[23] At a high ligand density, the arrangement of ligands is very compact. Therefore, it is easy for GM1 to cluster when there are many GM1 molecules in the lipid bilayer. If the number of GM1 molecules exceed the maximum value that the lipid bilayer can support, GM clusters. As a result, the CT binding ability is continuously weakened as the GM1 concentration increases. This process is illustrated in **Fig 3.13**. When the GM1 density is in a proper range, enough distance exists between each GM1 molecule, making it easy for CT to bind (**Fig.3.13 A**). However, at a high GM1 density (**Fig.3.13 B)**, less CT molecules will bind onto the lipid bilayer due to GM1 clustering.

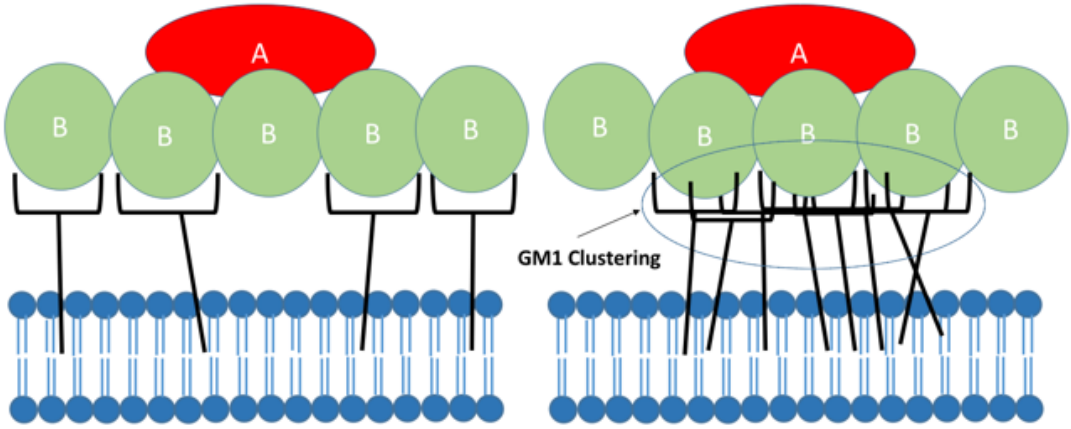

A B

Figure 3.13. (A) The concentration of GM1 is in a proper value, making it easy for CT to bind onto the lipid bilayer. (B) CT binding is inhibited by GM1 clustering on the DOPC bilayer.

3.6 Conclusion and Future Directions

This chapter studied the application of silica microsphere resonators in biomolecules detection. The Langmuir-Blodgett technique is a convenient method to transfer lipid bilayers onto the resonator surface. The silica microspheres coated with DOPC/GM1 bilayers were fabricated to detect the binding event of CT to GM1. This specific binding was confirmed by tracking the WGM resonant wavelength shifts. By changing the GM1 concentration and measuring WGM response, the maximum amount of GM1 supported by the DOPC bilayer can be estimated. Too much GM1 in the bilayer led to GM1 clustering, which inhibited CT-GM1 interaction and weakened the binding ability. In the future, it is necessary to further study the reasons for poor CT-GM1 binding at high GM1 concentrations. In addition, the value of the pressure used to form lipid bilayer may also effect molecule arrangement in the bilayer. Therefore, it is interested to study the pressure effect on the bilayer formation as well.

3.7 References:

1. Wolfbeis, O. S., Fiber-Optic Chemical Sensors and Biosensors. *Anal. Chem.* **2004,** *76* (12), 3269-3284.
2. Fan, X.; White, I. M.; Shopova, S. I.; Zhu, H.; Suter, J. D.; Sun, Y., Sensitive optical biosensors for unlabeled targets: A review. *Anal. Chim. Acta* **2008,** *620* (1-2), 8-26.
3. Vollmer, F.; Arnold, S., Whispering-gallery-mode biosensing: label-free detection down to single molecules. *Nat. Methods* **2008,** *5* (7), 591-596.
4. Zijlstra, P.; van der Molen, K. L.; Mosk, A. P., Spatial refractive index sensor using whispering gallery modes in an optically trapped microsphere. *Appl. Phys. Lett.* **2007,** *90* (16), 161101/1-161101/3.
5. François, A.; Reynolds, T.; Monro, T. M., A fiber-tip label-free biological sensing platform: a practical approach toward in-vivo sensing. *Sensors (Basel).* **2015,** 15(1), 1168–1181.
6. Pang, S.; Beckham, R. E.; Meissner, K. E., Quantum dot-embedded microspheres for remote refractive index sensing. *Appl. Phys. Lett.* **2008,** *92* (22), 221108/1-221108/3.
7. Arnold, S.; Khoshsima, M.; Teraoka, I.; Holler, S.; Vollmer, F., Shift of whispering-gallery modes in microspheres by protein adsorption. *Opt. Lett.* **2003,** *28* (4), 272-274.
8. Baaske, M. D.; Foreman, M. R.; Vollmer, F., Single-molecule nucleic acid interactions monitored on a label-free microcavity biosensor platform. *Nat. Nanotechnol.* **2014,** *9* (11), 933-939.
9. Saslowsky, D. E.; Kothe, M.; Lencer, W. I., Cholera toxin: Mechanisms of entry into host cells. *Top. Curr. Genet.* **2005,** *11* (Microbial Protein Toxins), 55-67.

10. Donowitz, M.; Welsh, M. J.; Johnson, J. R., Regulation of Mammalian Small Intestinal Electrolyte Secretion: Physiology of the Gastrointestinal Tract. *Raven Press*. **1987**, 2, 1351−1388.
11. Sharp, G. W. G.; Hynie, S. Stimulation of intestinal adenyl cyclase by cholera toxin. *Nature* **1971**, 229, 266−269.
12. Abdelmalak, B; Doyle, J. Anesthesia for otolaryngologic surgery. *Cambridge University Press.* **2013**, 282–287.
13. Spangler, B. D. Structure and function of cholera toxin and the related Escherichia coli heat-labile enterotoxin. *Microb. Rev*. **1992**, 56, 622−647.
14. Kuziemko, G. M.; Stroh, M.; Stevens, R. C., Cholera Toxin Binding Affinity and Specificity for Gangliosides Determined by Surface Plasmon Resonance. *Biochemistry* **1996,** *35* (20), 6375-84.
15. Fukuta, S.; Magnani, J. L.; Twiddy, E. M.; Holmes, R. K.; Ginsburg, V., Comparison of the carbohydrate-binding specificities of cholera toxin and Escherichia coli heat-labile enterotoxins LTh-I, LT-IIa, and LT-IIb. *Infection and Immunity*. **1988,** 56(7), 1748-53.
16. Masserini, M.; Freire, E.; Palestini, P.; Calappi, E.; Tettamanti, G., Fuc-GM1 ganglioside mimics the receptor function of GM1 for cholera toxin. *Biochemistry* **1992,** *31* (8), 2422-6;
17. Kuziemko, G. M.; Stroh, M.; Stevens, R. C., Cholera Toxin Binding Affinity and Specificity for Gangliosides Determined by Surface Plasmon Resonance. *Biochemistry* **1996,** *35* (20), 6375-84.
18. Choi, S.-K., *Synthetic Multivalent Molecules: Concepts and Biomedical Applications*. John Wiley & Sons: 2004; p 428 pp;

19. Mammen, M.; Chio, S.-K.; Whitesides, G. M., Polyvalent interactions in biological systems: implications for design and use of multivalent ligands and inhibitors. *Angew. Chem., Int. Ed.* **1998,** *37* (20), 2755-2794.

20. Kiessling, L. L.; Gestwicki, J. E.; Strong, L. E., Synthetic multivalent ligands as probes of signal transduction. *Angew. Chem., Int. Ed.* **2006,** *45* (15), 2348-2368.

21. Smith, E. A.; Thomas, W. D.; Kiessling, L. L.; Corn, R. M., Surface Plasmon Resonance Imaging Studies of Protein-Carbohydrate Interactions. *J. Am. Chem. Soc.* **2003,** *125* (20), 6140-6148.

22. Huskens, J.; Mulder, A.; Auletta, T.; Nijhuis, C. A.; Ludden, M. J. W.; Reinhoudt, D. N., A Model for Describing the Thermodynamics of Multivalent Host-Guest Interactions at Interfaces. *J. Am. Chem. Soc.* **2004,** *126* (21), 6784-6797.

23. Shi, J.; Yang, T.; Kataoka, S.; Zhang, Y.; Diaz, A. J.; Cremer, P. S., GM1 Clustering Inhibits Cholera Toxin Binding in Supported Phospholipid Membranes. *J. Am. Chem. Soc.* **2007,** *129* (18), 5954-5961.